AD-A145 935 FOLDED ACOUSTIC AND QUANTIZED OPTIC PHONONS IN SEMICONDUCTOR SUPERLATTICES(U) ILLINOIS UNIV AT URBANA LOOMIS LAB OF PHYSICS C COLVARD ET AL. JUL 84 1/1

UNCLASSIFIED ILL-(SS)-84-27 N00014-80-C-0701 F/G 12/1 NL

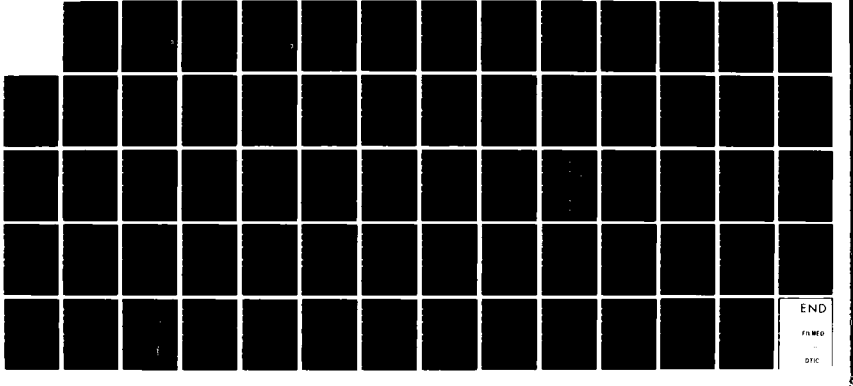

END

FILMED

DTIC

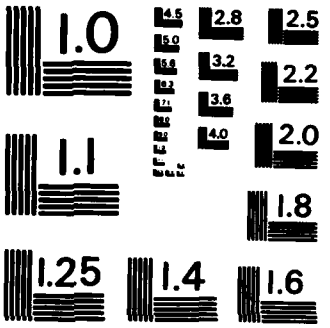

FOLDED ACOUSTIC AND QUANTIZED OPTIC PHONONS IN SEMICONDUCTOR SUPERLATTICES

By

C. Colvard, T. A. Gant, M. V. Klein

R. Merlin

R. Fischer, H. Morkoc

AND

A. C. Gossard

UNIVERSITY OF ILLINOIS AT URBANA-CHAMPAIGN

DEPARTMENT OF PHYSICS

LOOMIS LABORATORY OF PHYSICS

1110 W. GREEN STREET

URBANA, ILLINOIS 61801

P/84/6/84

ILL-(SS)-84-27
July 1984

FOLDED ACOUSTIC AND QUANTIZED OPTIC PHONONS IN SEMICONDUCTOR SUPERLATTICES

C. Colvard*, T. A. Gant, M. V. Klein†

Department of Physics and Materials Research Laboratory
University of Illinois at Urbana-Champaign (UIUC)
1110 W. Green St., Urbana, IL 61801

R. Merlin††

Materials Research Laboratory and Coordinated Science Laboratory
University of Illinois at Urbana-Champaign
Urbana, IL 61801

R. Fischer, H. Morkoc,

Department of Electrical Engineering & Coordinated Science Laboratory
(UIUC) Urbana, IL 61801

and

A. C. Gossard

AT&T Bell Laboratories
Murray Hill, NJ 07974

* Present address: Siemens Research & Technology Laboratories,
105 College Road East, Princeton, NJ 08540
† Also at Coordinated Science Laboratory, UIUC
†† Present Address: Department of Physics, University of Michigan,
Ann Arbor, MI 48109

PACS Index: 78.30.Gt
63.20.Dj
73.40.Lq
78.55.Ds

Typed by Cindy Elder

Abstract

Raman scattering studies of a variety of MBE-grown (GaAl)As superlattices are presented. Folded acoustic phonons appear as doublets in the Raman spectra. Their frequencies are accurately predicted by several models, including an approximate solution of an elastic continuum model through a perturbation approach. Scattering intensities of the folded acoustic modes are predicted by a photoelastic continuum model. Calculations on a layered dielectric continuum provide information about anisotropy of optical phonons. Linear chain model calculations indicate that optical phonons in binary superlattices are largely confined to alternate layers. Peaks in the Raman data are identified with the resulting quantized optic modes. It is shown that Raman scattering has the potential to provide structural information similar to that which can be obtained by x-ray diffraction.

I. INTRODUCTION

Semiconductor superlattices (SL's) have been of interest for nearly fifteen years now, an interest stimulated by the development of techniques, such as MBE and MOCVD, capable of growing crystals of alternating layers of two semiconductors with nanometer spatial periods. Potential device applications have spurred studies of the electronic properties of doped and undoped SL's and quantum well heterostructures. Much less attention has been paid to the vibrational properties, either theoretical or experimental. Calculations have been made for transverse phonon-polariton branches in a GaAs-AlAs SL[1], and discrete[2] and continuum[3] models have been used to describe phonon folding and to estimate surface mode behavior.[4] The creation of a gap in the acoustic phonon dispersion by the SL was first confirmed by acoustic transmission experiments.[5] Raman scattering, a natural probe for SL phonon studies, has been the most frequently employed experimental tool.

Manuel et al.[6] studied the resonant Raman behavior of LO-phonons near the energy gap of four GaAs-$Al_xGa_{1-x}As$ samples with 63Å < d < 200Å and $x \sim 0.25$. They also derived a two-dimensional result for the resonance behavior. An extensive study was made by Barker et al.[2] of Raman scattering and infrared absorption in a series of very thin layer GaAs-AlAs samples. They calculated the effects of phonon folding, and made comparisons between alloy samples and a number of thin layer SL's. Sai-Halasz et al.[7,8] noticed new peaks appearing between the LO^{GaAs} and LO_1^{AlGaAs} modes in resonant Raman spectra of GaAs-$Al_{.25}Ga_{.75}As$ samples which they attributed to umklapp processes. These new peaks were shown to be similar to E(LO) phonons by Merlin et al.[9] The first clear phonon-folding in light scattering experiments was seen by Colvard et al.[3] Later Raman studies report scattering from both acoustic[10,11] and optic[10] phonons, including resonant enhancements at quantized exciton levels.[12]

Brillouin scattering experiments have been performed by Sapriel et al.[11] Indications of optical phonon folding have been reported by Jusserand et al.[13]

We present here a comparison of experimental Raman scattering results from a variety of SL's with several theoretical models, including a perturbation calculation which reproduces the essentials of the acoustic phonon spectrum, such as sound velocity and gap widths. We show that Raman data can provide information on the layering parameters heretofore gathered primarily from x-ray diffraction. A model based on bulk photoelastic behavior is shown to predict the intensity of the observed folded acoustic phonon peaks. The optical phonons are seen to be best described by quantization, as in the electron case, rather than by zone folding.

In the next section, several models of SL phonon behavior are outlined. Section III presents a calculation of light scattering intensities, relating the folded phonon and Brillouin scattering intensity to the bulk photoelastic constants. Sections IV and V present the experimental results and discussion.

II. PHONON MODELS

Several different approaches to modelling superlattice phonons have been found to be useful, each having certain advantages. A linear chain model embodies the discrete nature of the crystal structure and provides information about evanescent behavior of optical phonons. It is most useful in frequency regions in which the bulk phonon dispersion is non-linear. At low frequencies and long wavelengths the lattice can be treated as an elastic continuum, in which case a Kronig-Penney type of approach yields a convenient analytic expression for phonon folding. The layer thicknesses in this case are not restricted to integral multiples of the monolayer spacing. Alternatively, at these same frequencies, the superlattice can be considered as a perturbation on an average elastic background. This approximate approach yields explicitly the gap widths and sound velocity for an arbitrary composition profile.

These models will be outlined below, in addition to a dielectric continuum model which allows an estimate of the effects of long-wavelength electric fields. Of course, one wants a comprehensive theory of superlattice effects which correctly deals with all microscopic short and long range forces. Such a theory is especially needed in dealing with the spectrum of optical phonons. Calculations using such a theory have recently been made by Yip and Chang.[14)]

A. Linear Chain Model

This model has been applied to binary-binary superlattices by Barker et al.[2)] It is valid in bulk crystals for phonons propagating along [001], where planes of atoms move as a whole, and the longitudinal and transverse vibrations are decoupled. For longitudinal modes a single nearest-neighbor spring constant provides the only free parameter, whereas two different nearest-

neighbor spring constants provide the anisotropy necessary to describe transverse vibrations.[2] These force constants are allowed to be different in GaAs and AlAs layers, and are fit to bulk values of either the LO(Γ) phonon frequency (or TO(Γ) and TA(X) for transverse modes) or the sound velocity v_{long} (or v_{trans} and TO(Γ) frequency). To fit both optic and acoustic regions, more distant neighbor interactions must be included.[15]

By utilizing bulk phonon solutions (propagating or evanescent) within the layers and matching these at the interfaces, arbitrary layer thicknesses can be considered by solving only a 4x4 determinant. The longitudinal case will be described here; the extension to anisotropic force constants for the transverse case is straightforward. Figure 1 shows the model used. Within each layer

$$M_1 \ddot{U}_1[m\varepsilon] = -K\,(2U_1[m\varepsilon] - U_2[m\varepsilon] - U_2[(m-1)\varepsilon]) \tag{1}$$

$$M_2 \ddot{U}_2[m\varepsilon] = -K\,(2U_2[m\varepsilon] - U_1[(m+1)\varepsilon] - U_1[m\varepsilon]) \tag{2}$$

where $U(m\varepsilon)$ is the displacement along $\hat{z}$ of the atom at $z = m\varepsilon$, and ε is the monolayer spacing $\varepsilon = a/2$. Taking $\pm\alpha$ as the phonon wavevector q_z in GaAs, this yields

$$\cos \alpha\varepsilon = \frac{(M_1\omega^2 - 2K)\,(M_2\omega^2 - 2K) - 2K^2}{2K^2}\,. \tag{3}$$

Defining $\gamma_{\pm} \equiv U_2/U_1$ for $\pm\alpha$, we find

$$\gamma_{\pm} = \frac{-K\,(1 + e^{\pm i\alpha\varepsilon})}{M_2\omega^2 - 2K}\,. \tag{4}$$

The above equations are for GaAs; similar expressions describe AlAs with wavevector $q_z = \pm\beta$ and $\delta_{\pm} \equiv U_2'/U_1'$. Eq. (3) is plotted in Fig. 2, which shows both the real and the imaginary part of q_z. The imaginary part indicates the rate of attenuation of a vibration at a particular frequency. For $\frac{a}{2} = 2.83\text{Å}$, a penetration depth of one monolayer for the amplitude U(z) corresponds to $\text{Im}(q_z) = 0.32\ \pi/(\frac{a}{2})$. The plot indicates that at GaAs optical mode frequencies the vibrations extend less than one monolayer into the AlAs, where they are damped optical modes with $\text{Re}(q) = 2\pi/a$. At AlAs optical frequencies they are even more localized in the AlAs layer, decaying into the GaAs as damped acoustical modes with $\text{Re}(q) = 0$. The result of this confinement of the optical vibrations is apparent in Fig. 3, where the folded superlattice optical modes are seen to be quite flat.

In a superlattice the displacements become $U_1(z) = Ae^{i\alpha z} + Be^{-i\alpha z}$ and $U_1'(z) = Ce^{i\beta z} + De^{-i\beta z}$. At an interface the forces must be matched, so that each wave behaves as if it were in an infinite medium. Thus at z = 0:

$$K[U_2(0) - U_1(0)] = K'[U_2'(0) - U_1'(0)] \tag{5}$$

and

$$K[U_1(\varepsilon) - U_2(0)] = K'[U_1'(\varepsilon) - U_2'(0)]. \tag{6}$$

With the help of Eq. (1) this gives

$$U_2(0) = U_2'(0) \tag{7}$$

and

$$K[U_1(\varepsilon) - U_1(0)] = K'[U_1'(\varepsilon) - U_1'(0)] \tag{8}$$

which are the discrete analogs of the requirements that displacement and

stress be continuous at an acoustical boundary. Similarly, at $z = n\varepsilon$ we have

$$U_2(n\varepsilon) = U_2'(n\varepsilon) \tag{9}$$

and

$$K[U_1(n\varepsilon + \varepsilon) - U_1(n\varepsilon)] = K'[U_1'(n\varepsilon + \varepsilon) - U_1'(n\varepsilon)]. \tag{10}$$

Imposing the periodic requirement that $U_{SL}(z+d) = U_{SL}(z)\, e^{iqd}$, where q is the superlattice wavector, and setting layer thicknesses $d_1 + d_2 = d$, gives the set of equations:

$$\gamma_+ A + \gamma_- B = \delta_+ C + \delta_- D \tag{11a}$$

$$G_+ A + G_- B = H_+ C + H_- D \tag{11b}$$

$$\gamma_+ A e^{-i\alpha d_1} e^{iqd} + \gamma_- B e^{i\alpha d_1} e^{iqd} = \delta_+ C e^{i\beta d_2} + \delta_- D e^{-i\beta d_2} \tag{11c}$$

$$G_+ A e^{-i\alpha d_1} e^{iqd} + G_- B e^{i\alpha d_1} e^{iqd} = H_+ C e^{i\beta d_2} + H_- D\, e^{-i\beta d_2} \tag{11d}$$

where

$$G_\pm \equiv K(e^{\pm i\alpha\varepsilon} - 1) \tag{12a}$$

and

$$H_\pm \equiv K'(e^{\pm i\beta\varepsilon} - 1) \tag{12b}$$

The solution of these equations is given by

$$\cos qd = \cos \alpha d_1 \cos \beta d_2$$

$$+ \frac{2(\gamma_+\gamma_-H_+H_- + \delta_+\delta_-G_+G_-)}{(\gamma_-\delta_-G_+H_+ + \gamma_+\delta_+G_-H_- - \gamma_-\delta_+G_+H_- - \gamma_+\delta_-G_-H_+)} \sin \alpha d_1 \sin \beta d_2 \qquad (13)$$

In the transverse case, an additional term appears in the sine multiplicand. This solution is shown in Fig. 3 for a (5,4) superlattice. The phonon branches above the first but below about 200 cm^{-1}, although strictly optical branches of the SL, are commonly referred to as folded acoustic branches due to their origin in the bulk acoustic phonons.

B. Elastic Continuum Models

The phonon dispersion is approximately linear below about 100cm^{-1} for LA phonons and below 50 cm^{-1} for TA phonons, and in this region the crystal can be treated as an elastic continuum. Vibrations in layered elastic media have been considered by Rytov[16], and his results have been shown to apply to acoustic phonons in superlattices.[3] The dispersion is given by

$$\cos qd = \cos\left(\frac{\omega d_1}{v_1}\right) \cos\left(\frac{\omega d_2}{v_2}\right) - \frac{1 + \kappa^2}{2\kappa} \sin\left(\frac{\omega d_1}{v_1}\right) \sin\left(\frac{\omega d_2}{v_2}\right) \qquad (14)$$

which is a solution of the wave equation

$$\ddot{\rho U} = \frac{\partial}{\partial z}\left(K \frac{\partial U}{\partial z}\right). \qquad (15)$$

Here the sound velocity is $v = (K/\rho)^{1/2}$ in each layer, and $\kappa \equiv \rho_2 v_2/\rho_1 v_1$. In the limit of large wavelengths, the superlattice sound velocity $v_{SL} = \omega/q$ becomes

$$v_{SL} = d\left[\frac{d_1^2}{v_1^2} + \frac{d_2^2}{v_2^2} + \left(\kappa + \frac{1}{\kappa}\right)\frac{d_1 d_2}{v_1 v_2}\right]^{-\frac{1}{2}} . \tag{16}$$

If the elastic constants are equal in the two layers, this reduces to

$$v_{SL} = (\langle v^{-1}\rangle_{rms})^{-1}. \tag{17}$$

The above Rytov solution is valid for a square-wave-like compositional modulation with sharp interfaces. Its results can be recovered, and extended to arbitrary composition profiles, by a perturbation approach. We replace Eq. (15) by

$$\frac{\partial}{\partial z}\left[(K_o + \Delta K)\frac{\partial U}{\partial z}\right] + (\rho_o + \Delta\rho)\,\omega^2 U = 0 \tag{18}$$

where K_o and ρ_o are the zeroth Fourier components of the elastic constant and density, and $\Delta K(z)$ and $\Delta\rho(z)$ describe the compositional variation. They depend upon the local Al concentration x. The lowest order equation is then

$$\frac{K_o}{\rho_o}\frac{\partial^2 U}{\partial z^2} + \omega^2 U = 0 \tag{19}$$

which gives a virtual crystal sound velocity $v_o^2 \equiv K_o/\rho_o$. This agrees with Eq. (17) for equal elastic constants.

We can make the expansions

$$U(z) = \sum_q U_q\, e^{iqz} \tag{20a}$$

$$\Delta K = \sum_S K_S e^{iSz} \tag{20b}$$

$$\Delta\rho = \sum_S \rho_S e^{iSz} \tag{20c}$$

where S is a reciprocal lattice vector, $S = 2\pi m/d$, and q ranges over the bulk Brillouin zone. Eq. (18) then becomes

$$(v_o^2 q^2 - \omega^2)\, U_q + \sum_S \frac{1}{\rho_o} \left[q(q-S)\, K_S - \omega^2 \rho_S\right] U_{q-S} = 0. \tag{21}$$

The ω^2 in the perturbation term in Eq. (21) can be approximated by

$$\omega^2 \approx v_o^2\, |q(q-S)|. \tag{22}$$

This allows the perturbation to be written as $V_S\, q(q-S)$, where we define $V_S \equiv (K_S \mp v_o^2\, \rho_S)/\rho_o$. The -(+) sign applies if $q(q-S)$ is positive (negative). We keep only the terms in the sum which correspond to states that are strongly mixed by the perturbation, i.e., for which

$$|v_o^2 q^2 - v_o^2 (q - S)^2| \lesssim |q(q-S) V_S|. \tag{23}$$

This is true for the states U_q and U_{q-S} where $S \approx 2q$. Considering only these two terms, we can simplify Eq. (21) and obtain

$$\omega^2 = \frac{v_o^2}{2} \left[q^2 + (q-S)^2\right] \pm \left[\frac{v_o^4}{4} (q^2 - (q - S)^2) + |V_S|^2 q^2 (q-S)^2\right]^{1/2}, \tag{24}$$

which for exact degeneracy, $S = 2q$, becomes

$$\omega^2 = v_o^2 q^2 \pm |V_S|\, q\, (q-S). \tag{25}$$

If we set $q = \frac{m\pi}{d}$ then

$$\omega^2 = (v_o^2 \pm |V_S|) \frac{\pi^2 m^2}{d^2} \tag{26}$$

gives the frequencies on either side of a gap, at the SL zone edge for m odd and zone center for m even. Taking ρ_S for a square wave, and assuming $K_S = 0$ (i.e. K equal in the two layers), we find

$$|V_S| = |\frac{v_o^2(\rho_b - \rho_a)}{\rho_o \pi m} \sin (\frac{m\pi d_1}{d})|, \tag{27}$$

where ρ_a and ρ_b are the densities in the two layers, and where

$$\rho_o = d^{-1}(d_1\rho_a + d_2\rho_b). \tag{28}$$

The expected gaps are found by noting that

$$\omega_+ - \omega_- = \frac{|V_S|}{v_o} \frac{\pi|m|}{d} \tag{29}$$

which gives, again for constant K and sharp boundaries,

$$\omega_+ - \omega_- = |\frac{v_o(\rho_b - \rho_a)}{\rho_o d} \sin (\frac{m\pi d_1}{d})|. \tag{30}$$

C. Dielectric Continuum Model

For layers thick enough that a local dielectric constant is a well defined quantity, the optical phonon behavior can be surmised by treating the SL as a layered dielectric continuum. The dielectric constant can be

represented in the binary layers by

$$\varepsilon(\omega) = \varepsilon_\infty\left(1 + \frac{\omega_L^2 - \omega_T^2}{\omega_T^2 - \omega^2 - i\omega\Gamma}\right) \tag{31}$$

which for zero damping becomes

$$\varepsilon(\omega) = \varepsilon_\infty \left(\frac{\omega_L^2 - \omega^2}{\omega_T^2 - \omega^2}\right) . \tag{32}$$

In the alloy we can use the factorized form[17]

$$\varepsilon(\omega) = \varepsilon_\infty \frac{(\omega_{L1}^2 - \omega^2)\ (\omega_{L2}^2 - \omega^2)}{(\omega_{T1}^2 - \omega^2)\ (\omega_{T2}^2 - \omega^2)} \tag{33}$$

where ω_L and ω_T are the long wavelength longitudinal and transverse phonon frequencies. The subscripts 1 and 2 refer to the composition dependent two-mode behavior of the alloy. Maxwell's equations can then be solved for polarization waves propagating parallel or perpendicular to the layers in the $q \to 0$ limit. This has been done in the absence of phonon dispersion by Rytov.[18]

The results can most conveniently be summarized by noting that, for long waves, the superlattice behaves like a homogeneous, anisotropic crystal. The average dielectric constants are found to be

$$\varepsilon_{x,y} = \bar{\varepsilon} = d^{-1}(d_1\varepsilon_1 + d_2\varepsilon_2) \tag{34}$$

$$\varepsilon_z = \overline{(\varepsilon^{-1})}^{-1} = d\varepsilon_1\varepsilon_2(d_1\varepsilon_2 + d_2\varepsilon_1)^{-1} \tag{35}$$

with ε_1 and ε_2 given by Eqs. (32) or (33).

The zeroes and poles of these dielectric constants occur at the longitudinal and transverse frequencies of the composite layered structure, corresponding respectively to the vanishing of the average displacement $\bar{D}$ or electric field $\bar{E}$. For polarization in the plane of the layers and $\vec{q}$ along the $\hat{z}$ direction, the poles of Eq. (34) give TO modes of E-symmetry at the bulk TO frequencies. For polarization parallel to the superlattice axis, the zeroes of Eq. (35) give LO modes of B_2- or A_1-symmetry at the bulk LO frequencies. In both cases the polarization, and electric field where non-zero, exists only in the layer at whose normal frequency the vibration occurs. If phonon dispersion is considered, these modes are the quantized optic phonons due to SL zone folding.

For $\vec{q}$ in the layer plane two new modes appear, a B_2(TO)-like mode at the poles of Eq. (35) and an E(LO)-like mode at the zeroes of Eq. (34). The solutions are given by

$$\frac{\varepsilon_1(\omega)}{\varepsilon_2(\omega)} = -\frac{d_1}{d_2} \qquad B_2(TO) \qquad (36a)$$

$$-\frac{d_2}{d_1} \qquad E(LO) \qquad (36b)$$

with Eqs. (32) or (33) for ε_1 and ε_2. These frequencies occur between the bulk ω_L and ω_T. For $qd > 0$ the polarization decays exponentially away from interfaces, but in the thin layer limit it is nearly constant throughout the superlattice. Figure 4 plots the frequencies of these modes versus layer thickness for a GaAs-AlAs superlattice. Note that if $d_1 >> d_2$, the LO-mode can occur at the TO-frequency and vice-versa.

Solutions will also exist at the bulk LO and TO frequencies for modes propagating along the layers but spatially quantized along $\hat{z}$. Ignoring polariton effects, these modes will be similar to the quantized bulk phonons mentioned above at the wavevectors accessible to Raman scattering.

III. Photoelastic Mechanism for Light Scattering

At laser energies far from resonance with superlattice electronic transitions, light scattering from the folded acoustic phonons can be treated as a coherent sum of scattering within bulk-like layers due to the photoelastic effect. The photoelastic coefficient is taken to be a function of position z; its value depends on the local Al concentration x:

$$P(z) = \frac{dP}{dx}\, x(z). \tag{37}$$

If the interfaces are abrupt, this will be a square wave:

$$P(z) = \begin{cases} P_a & 0 \le z < d_1 \\ P_b & d_1 \le z < d = d_1 + d_2 \end{cases} \tag{38}$$

The strain due to an LA phonon will cause a proportionate change in the susceptibility:

$$\delta\chi(z) = P(z)\, \frac{\partial U(z)}{\partial z}\,. \tag{39}$$

Light will be scattered by the q^{th} component of this susceptibility fluctuation that conserves momentum, $\vec{q} = \vec{k}_i - \vec{k}_s$, as in ordinary Brillouin scattering:[19)]

$$I(\omega) \propto \langle\, |\delta\chi_q|^2 \,\rangle_\omega. \tag{40}$$

This component is given by

$$\delta\chi_q = \int_{-\infty}^{\infty} e^{-iqz} P(z)\, \frac{\partial u(z)}{\partial z}\, dz. \tag{41}$$

In the Kytov model, away from gaps in the phonon dispersion curves, this integrand is

$$\delta\chi(z) = \begin{cases} i\alpha P_a e^{i\alpha z} U_{oa} & 0 < z < d_1 \\ i\beta P_b e^{i\beta z} U_{ob} & d_1 < z < d_2 \end{cases} \tag{42}$$

where $\alpha = \frac{\omega}{v_1}$, $\beta = \frac{\omega}{v_2}$ and $v_{1,2}$ are bulk sound velocities. For simplicity the difference between α and β can be ignored, $\alpha \approx \beta \approx q_z$ and $U_{oa} \approx U_{ob}$. P(z) can be separately expanded

$$P(z) = \sum_m P_m e^{iS_m z}, \quad S_m \equiv \frac{2\pi m}{d} \tag{43}$$

allowing the Raman tensor to be written

$$\delta\chi_q = \sum_m P_m \, i(q - S_m) \, u_{q-S_m}. \tag{44}$$

The $\pm$ m terms in this sum describe Raman scattering from folded LA phonons at $\omega_m = |q \mp S_m| v_{SL}$ with intensity

$$I_m \propto \omega_m (n_m + 1) \, |P_m|^2. \tag{45}$$

(Here n_m is the Bose factor). For m = 0 this gives the Brillouin scattering cross section in a superlattice at $\omega = q \, v_{SL}$. For the square wave case of Eq. (38)

$$P_0 = \frac{1}{d} (d_1 P_a + d_2 P_b), \tag{46}$$

$$P_m = \frac{i(P_b - P_a)}{2\pi m} \left[1 - \exp(-i2\pi m d_1/d)\right], \quad m \neq 0, \tag{47}$$

giving

$$|P_m|^2 = \left|\frac{(P_b - P_a)}{m\pi} \sin\left(\frac{m\pi d_1}{d}\right)\right|^2 \quad m \neq 0. \tag{48}$$

For propagation along $\hat{z}$ and backscattering from a (001) face, only LA phonons can be seen, these through the component $P^{xxzz} = P^{12}$ in cubic crystals. Thus the scattered folded phonon intensity can be compared with that for the Brillouin scattering:

$$I_m/I_{Brill} = \frac{(P_b^{12} - P_a^{12})^2}{P_0^2} \frac{\sin^2(m\pi d_1/d)}{\pi^2 m^2} \eta \tag{49}$$

The factor η accounts for the frequency difference between ω_m and ω_{Brill}, $\eta = [\omega_m(n_m + 1)]/[\omega_0(n_0 + 1)]$. For $\hbar\omega_m \ll kT$, $\eta \approx 1$.

Ren and Harrison have calculated photoelastic constants for GaAs and AlAs.[20] As defined here, their values give $P^{12} = 0.48$ in GaAs and 0.05 in AlAs for the change in χ with strain. For $d_1 = d_2 = d/2$, this gives

$$I_1/I_{Brill} \approx 0.3 .$$

IV. Experimental

All samples used in this study were grown by molecular beam epitaxy on [001] oriented GaAs substrates. Periods range from 20Å to 200Å, and SL thicknesses vary between 0.5μ and 4μ. Specific SL's will be referred to by their composition. The notation used for an $Al_yGa_{1-y}As$-$Al_xGa_{1-x}As$ SL will be $(d_1;y,d_2:x)$, where d_1 and d_2 are layer thicknesses. If no value of y is

specified, as in most samples, the first number refers to pure GaAs layers ($y = 0$).

Light from a cw Ar^+, Kr^+, or dye laser was used to illuminate the samples, which were held in a He cryostat at temperatures between 2-300K. Scattered light was analyzed by a double pass 3/4 meter spectrometer equipped with 1800 g/mm holographic gratings and was detected by an RCA C31034A photomultiplier tube operated in phonon-counting mode. An Apple II-plus computer was used to collect data and control the experiment. Most measurements were made with light incident at an angle close to Brewster's angle, polarized in the plane of incidence. Scattered light was collected with an f/1.4, 85 mm focal length lens whose axis was normal to the surface of the sample. Successive rotations of a polarizer in the scattered beam allowed polarized and depolarized spectra to be interspersed in the same spectral scan, so that small frequency shifts between the two spectra could be detected.

Pieces of one (41Å, 8Å:1) sample were annealed at 850°C for times from 0.25 to 16 hours. During the anneals, the samples were placed between two pieces of GaAs in an atmosphere of flowing forming gas inside a quartz furnace. No visible surface degradation or increased surface scattering was seen after annealing for up to 16 hours.

V. Results and Discussion

A. Acoustic Region (5-220cm^{-1})

In this region are seen the most striking features of a superlattice spectrum: the folded acoustic phonons. They appear as doublets in the A_1 spectrum at frequencies from 5 to 100cm^{-1}. An example is seen in Fig. 5, which exhibits three folded orders, as shown in the inset. The data are taken from a (42Å, 8Å:.3) sample. Observation of small peaks close to the laser line is greatly aided by the quality of the MBE-grown sample surface. Peaks as low as 7cm^{-1} have been clearly seen. At these small shifts, the intensity of the light scattering is enhanced by the thermal factor n + 1, which at room temperature is 21.5 at 10cm^{-1}, compared to 1.3 at the 292cm^{-1} GaAs LO phonon frequency. The data presented here include this factor, which must be kept in mind when interpreting relative intensities.

Figure 6 shows some further examples of the folded doublets, all spectra taken out of resonance at 5145Å. The widths of the peaks are quite small, usually 2 to 3 cm^{-1}, including an instrumental linewidth of about 2cm^{-1}. The expected contribution to the width due to absorption broadening of q is less than 0.5cm^{-1}. The acoustic phonons apparently experience a well defined average period, and show little inhomogeneous broadening. Also seen in the spectra is the well known 2TA structure, which peaks at 160cm^{-1} in GaAs and at about 200cm^{-1} in AlAs. After correcting for the n + 1 Bose factor, we find that the intensity of the first folded peak varies from 0.01 to 0.13 times the allowed GaAs LO intensity in the samples studied, averaging about 0.05. Under resonant enhancement these two intensities can become comparable.

As pointed out in the previous section, the folded doublets correspond to scattering from acoustic phonons with wavevectors $2\pi m/d \pm q$. For frequencies away from the gaps, i.e., where the acoustic dispersion is linear, these

longitudinal modes are running waves with equal components of A_1 and B_2 character. Light scattering from the Raman-active A_1 component gives equal intensities for the members of each doublet.[11] This can be seen in the lower curves of Fig. 6. The upper curves show the relative intensities of the doublets becoming progressively more unequal in samples with smaller periods. This indicates some admixture of a standing wave due to Bragg reflection and the opening of a gap in the dispersion curve. Figure 7 illustrates the first zone-center gap in a (5,4) superlattice. The solid curve is from a calculation using the linear chain model, which fits the bulk sound velocity of GaAs with the spring constant being the only adjustable parameter. The data points were taken from a sample with 25.5Å period by varying the laser wavelength from 4579Å to 6764Å. In such thin period samples, the wavevector transfer q is just barely in the region where the dispersion begins to flatten out into the gap. In the case of thicker GaAs layers, i.e. $d_1 > d_2$, the upper curve takes on B_2 symmetry, the lower one A_1 symmetry. Because in acoustic modes the atoms in a unit cell move in phase, the B_2 mode is effectively of odd symmetry under inversion. This gives a vanishing cross-section, since purely odd modes cannot ordinarily participate in Raman scattering. One can predict that small period samples having $d_1 < d_2$ will display the opposite asymmetry, the lower frequency peak having mostly B_2 symmetry and thus being weaker.

The wavevector transfer in backscattering is too large to truly probe the folded gap. In forward scattering, although q_z can be made small, spurious laser light can overwhelm data taken at small frequency shifts. Another possible way to study the gaps is to make samples with large enough period so that $q_z = 4\pi n/\lambda_L \simeq \frac{\pi}{d}$, allowing scattering from the zone-edge gap. This would require $d \simeq 250$Å at $\lambda_L = 4579$Å in a sample with $n \simeq 4.5$, well within the realm of current technology.

The data presented thus far are all on longitudinal phonons. Some folded transverse phonons have been seen in a Brewster angle scattering geometry. Figure 8 shows an example. The transverse phonons labeled by T appear in both (x,x) and (x,y) spectra. They have E symmetry in the superlattice, and are seen due to the deviation from true backscattering.

A comprehensive confrontation of theory vs. experiment for the folded phonon frequencies is difficult, considering the variety of periods, layer thickness ratios, and alloy compositions studied. In addition, the bulk sound velocity in AlAs is not well known. It is often estimated (as here) by $v_s^2 = C/\rho$, using the same elastic constant C as in GaAs. (The values of elastic constants $C_{11} = 12.5$, $C_{12} = 5.34$, and $C_{44} = 5.42 \times 10^{11} dyn/cm^2$ are given in reference 20 for AlAs, estimated from empirical relations and typical III-V values. This C_{11} is 6% larger than in GaAs). Figure 9 gives a plot of the folded phonon frequencies observed vs. inverse period. The shaded bands indicate the frequencies expected for the first three foldings of an average linear acoustic branch. They are bounded by $\omega_{\pm} = v_{\pm}(2\pi m/d)$, where v_+ is the sound velocity of AlAs, v_- that of GaAs. The midpoint of each doublet is expected to lie within such a band, its exact position depending on the Al to Ga ratio in the sample. The doublets off to the lower right represent transverse phonons.

The doublet splitting is seen to be $\sim 5cm^{-1}$ in all observed cases. This is consistent with the wavevector transfer $q = 4\pi n/\lambda_L$ for backscattering. The phonon doublets are at $\omega = v_{SL}(S_m \pm q)$ giving

$$\Delta\omega = 2v_{SL}q = 8\pi n v_{SL}/\lambda_L \tag{50a}$$

$$\approx 5cm^{-1}. \tag{50b}$$

It is felt that the scatter in the data is largely due to uncertainty in the value of the sample period. When this was not determined by x-ray diffraction, it was estimated from growth conditions. Furthermore, a sample's period can vary across its surface. Figure 9 demonstrates the ability of Raman scattering in a superlattice to provide structural information, similar to that from x-rays, by measuring the sample period. It has the advantage of providing convenient spatial resolution as well.

Another feature of interest in Fig. 9 is the appearance of two samples showing m = 1 and m = 3 phonon doublets, but none with m = 2. Figure 10 presents data from sample (41Å,41Å:0.3). The inset is a dispersion calculation, using the Rytov model, with the observed peaks indicated. Missing peaks are also seen in the data of Figure 11 on a (85Å,88Å:0.3) sample. The inset corresponds to the lower curve, taken out of resonance at λ_L = 5145Å. (Note, incidentally, that the data are taken with q over halfway into the superlattice Brillouin zone.) These data lend support to the model of photoelastic scattering presented in section 2. Both samples have nearly equal layer thicknesses; Eq. (48), along with Eq. (45), shows that in this case the scattering vanishes for even values of m. The x-ray diffraction data in Fig. 12 were taken from this sample. Here also the second satellite is missing, corroborating these results. In the samples studied, the ratio of the intensity of the m = 1 peak to that of the m = 2 peak is generally consistent with Eq. 45, after corrections are made for the thermal factor in Eq. (45). The intensities of the second and third peaks in Fig 5 fall off slightly faster than predicted, presumably due to the sensitivity of $\sin^2(\pi m d_1/d)$ to the exact layer thicknesses, especially for larger m.

To see the effect of a non-sharp interface, several pieces of sample (41Å,8Å:1), which contains pure AlAs barrier layers, were annealed at 850°C for

several intervals, up to 16 hours. This causes the interfaces to diffuse.[21] The effect on the folded phonons is seen in Fig. 13. The intensity decreases, while the frequency and width (within the experimental limits) do not change. This agrees with predictions of the photoelastic scattering model. The background at frequencies below that of the phonons also decreases. The data were taken at room temperature and are normalized to 50 counts/s at $265cm^{-1}$ (the TO(GaAs) peak). No significant increase was seen in disorder activated scattering (DALA and DATA).

Under resonant conditions the intensity of the folded phonon scattering can be significantly altered. An example is the upper curve of Fig. 11, taken near the $E_o + \Delta_o$ gap of the superlattice. The even-m phonons are now seen, but the peaks are asymmetric, and they are shifted in a way that cannot be explained entirely by a shift in q. Resonance of the laser photon with excitation to a particular SL state, which is an appropriate combination of bulk propagating and evanescent states in the two layers, invalidates the assumptions of Section III. The asymmetry suggests a coupling between the discrete phonons and a background continuum. Although not pursued here, other examples of such a coupling have been seen, as in Fig. 14. The features near $32cm^{-1}$ appear to be anti-resonances associated with acoustic phonons at the SL zone edge, at half the frequency of the sharp zone center m = 1 peaks. The bump at 100 cm^{-1} is due to second order optical phonon difference scattering at $\omega_{LO}(AlAs)-\omega_{LA}(GaAs)$.

Not all samples studied show the sharp folded phonons and low background that we consider to be indicative of high quality growth. Figure 15 shows data from three samples whose Raman spectra are dominated by disorder-activated scattering. The lower two curves are from samples (14Å:0.5, 14Å:1) and (38Å:0.25, 13Å:1), which contain no pure GaAs layers. DALA and DATA

structure is also seen in samples with thick AlAs layers, as in Fig. 16. This implies that the disorder which relaxes the momentum conservation does not arise solely within alloy layers, but may be more generally related to the difficulty of growing high quality layers with high Al content.

B. Optic Region (220-420cm^{-1})

Due to the two-mode behavior of $Al_xGa_{1-x}As$ alloys, the effect of layering on phonons near the GaAs optical frequency in GaAs-$Al_xGa_{1-x}As$ SL's will depend strongly upon the value of x in the barrier layers. For $x < 1$ both layers may support GaAs-like optical vibrations, resulting in a dispersive ω vs. q with small gaps. In this case, the normal mode may have a different number of nodes in the two layers. For AlAs-like vibrations, and for GaAs-like vibrations in samples with $x \approx 1$, the phonons are highly damped in the non-propagating layer. As indicated in Fig. 2, these damped modes are optic-like [$Re(q) = \pi/(a/2)$] in AlAs layers and acoustic-like (q purely imaginary) in GaAs layers. The localization in alternate layers produces flat optical branches. Whereas Brillouin zone folding adequately describes the effect of SL layering on the acoustic phonons, the optic branches are better regarded as spatially quantized, analogous to the quantization of electrons in potential wells.

Figure 17 shows data from four GaAs-AlAs samples with GaAs layer thickness increasing from top to bottom. The dominant peaks occur in the (x,y) geometry, indicating they have B_2 symmetry. TO phonons occur in both (x,x) and (x,y) at ~ 265cm^{-1} and ~ 357cm^{-1}. In the upper two curves, weak A_1 symmetry peaks are seen in (x,x). These two samples have been studied under resonant conditions. Figure 18 shows a more detailed spectrum of sample (20Å, 12Å:1), taken near the band gap. Two peaks are seen in each geometry, in addition to the TO phonon.

The resonant behavior of these phonons is given in Fig. 19. The data were taken with λ_L = 6765Å by varying the temperature between 100K and 300K. The temperature dependence of all peak frequencies, $-0.015 cm^{-1}/K$, agrees with that of GaAs. The luminescence peak at an energy of 1.805 eV at 300K was used to monitor the change in band gap. Both the TO phonon and peak 3 show little resonance enhancement. Peaks 2 and 4 resonate together, reaching a maximum 20 meV above that of peak 5.

Sample (14Å, 12Å:1) shows a similar optical phonon structure and resonance behavior, except that peaks 2 and 4 shift to higher frequencies with lower exciting energies (as the laser is tuned through the band gap), and their resonance maximum is about 50 meV higher than that of peak 5.

A simple prediction of the quantized frequencies is difficult for lack of a good model. An upper limit for confinement-induced shifts can be obtained by regarding the bulk LO dispersion as

$$\omega^2 = \omega_L^2 - v_s^2 q^2 \tag{51}$$

where v_s is the longitudinal sound velocity. This is the small q limit of a linear chain model, but it overestimates the dispersion. The folded frequencies are then given by

$$\omega^2 = \omega_L^2 - v_s^2 \left(\frac{\ell\pi}{d_1}\right)^2 \tag{52}$$

where ℓ is the folding order and d_1 is the single layer thickness. Using the exact linear chain, we find the result to be somewhat less dispersive, but it is still not accurate enough, giving an uncertainty of several cm^{-1} depending on the fitting parameters. The existing neutron data on GaAs LO phonon

dispersion[23] disagree with Raman results by $6cm^{-1}$ at q = 0; they imply a nearly flat LO branch out to one third of the bulk zone edge.

Figure 20 is a plot of observed optical phonon frequencies in the binary layer samples. The straight lines are from Eq. (52), using bulk values of v_s and ω_L, for several values of ℓ. Note that ω^2 is plotted vs. inverse squared layer thickness. Peaks not otherwise indicated appear in the B_2-allowed (x,y) geometry. Peaks labeled by E have been previously assigned to E-symmetry phonons, as mentioned below. Points along the lower edge of both regions corresond to TO phonons.

The thickness dependence of the highest B_2 mode frequencies is rather well described by the ℓ = 1 line. These include the peak labeled 5 in Fig. 18. The dotted arrows suggest that the deviation shown by sample (11Å, 10Å:1) from this line may be due to an incorrect determination of its relative layer thicknesses. Keeping d constant but adjusting d_1/d_2 takes the triangles into the crosses. X-ray diffraction provides a precise determination of superlattice period from the satellite spacing. The measurement of individual layer thicknesses can be done by Fourier analysis of satellite intensities or by estimating the average aluminum content from the average lattice constant. The x-ray data are sometimes not good enough to do this accurately. As pointed out in connection with Fig. 14, a good understanding of phonon folding can allow Raman scattering to provide this structural information.

The remaining peaks between the highest frequency B_2 mode and the TO mode are difficult to assign. A rough correlation exists between the ℓ = 2 line and the second B_2 peak. Consideration of the mode symmetries, and the fact that Eq. (52) overestimates the dispersion, suggest that the A_1 mode labeled 4 in Fig. 18 should corresponds to ℓ = 2. The second B_2 peaks, labeled 3 in the previous figure, then corresponds to ℓ = 3.

Previous reports[9] have suggested the E symmetry modes propagating parallel to the interfaces may appear in backscattering spectra due to disorder. Such modes have yet to be systematically verified, although such scattering may contribute to the structure typified by Fig. 18. No additional optical phonon peaks were seen in any of the alloy-barrier samples included in this study, as were seen in earlier studies. This may be due to the high quality of the present interfaces.

The interfaces in sample (41Å, 8Å:1) were intentionally blurred by annealing, and the optical frequency data are presented in Figs. 21 and 22. The curves were taken in the (x,y) geometry and are normalized to 50 counts/s at 265cm^{-1} (TO phonon). Pieces of the sample were annealed for 0.25, 1, 4, 9 and 16 hours at 850°C. The LO phonons are seen to shift toward lower frequency, and a low frequency tail appears on the TO phonon. The data are approaching the average alloy spectrum with increasing annealing. For an average Al concentration of x = 0.16, confirmed in this sample by x-ray diffraction,[24] the alloy LO peaks are expected at 285 and 370cm^{-1}.[17] The LO phonon in Fig. 37 has moved below this value to 281cm^{-1}, perhaps indicating a superlattice effect. Even after 16 hours the composition profile should remain sine-like.[22] No trace of the behavior of an x = .5 alloy is seen, which might be expected from equal interpentration at an interface. This would give peaks at 271 and 388cm^{-1}.

In summary, we have examined several models for phonon behavior in semiconductor SL's, and have compared these with Raman scattering data from a number of aluminum gallium arsenide based SL samples. The models describe well the data in the acoustic phonon region. A photoelastic approach describes the Raman intensities from folded phonon doublets. The Raman data are shown to provide structural information similar to that gained from x-ray

diffraction. In the optic region, the correspondence between the models and data is not as good. The behavior of the optic modes seems to be best described in terms of quantized levels, similar to confined electrons, due to confinement within one type of layer. This confinement depends of course on the alloy concentration and phonon frequency, due to two-mode behavior. Better theories, which include the effects of electric fields, are needed to describe the optical behavior.

Acknowledgements

We thank S. L. Cooper, D. A. Neumann and H. Zabel for providing x-ray diffraction data. This work was supported by NSF DMR 82-03523 and 80-20250, ONR N00014-80-C-0701, JSEP under N-00014-79-C-0424, and AFOSR under F49620-83-K-201.

REFERENCES

1. R. Tsu and S. S. Jha, Appl. Phys. Lett. 20, 16 (1972).

2. A. S. Barker, Jr., J. L. Merz, and A. C. Gossard, Phys. Rev. B17, 3181 (1978).

3. C. Colvard, R. Merlin, M. V. Klein, and A. C. Gossard, Phys. Rev. Lett. 45, 298 (1980).

4. J. Sapriel, B. Djafari-Rouhani, and L. Dobrzynski, Surf. Sci. 126, 197 (1983).

5. V. Narayanamurti, H. L. Störmer, M. A. Chin, A. C. Gossard, and W. Wiegmann, Phys. Rev. Lett. 43, 2012 (1979).

6. P. Manuel, G. A. Sai-Halasz, L. L. Chang, C.-A. Chang, and L. Esaki, Phys. Rev. Lett. 37, 1701 (1976).

7. G. A. Sai-Halasz, A. Pinczuk, P. Y. Yu, and L. Esaki, Solid State Commun. 25, 381 (1978).

8. G. A. Sai-Halasz, A. Pinczuk, P. Y. Yu, and L. Esaki, Surf. Sci. 73, 232 (1978).

9. R. Merlin, C. Colvard, M. V. Klein, H. Morkoc, A. Y. Cho, and A. C. Gossard, Appl. Phys. Lett. 36, 43 (1980).

10. C. Colvard, R. Merlin, M. V. Klein, and A. C. Gossard, Journal de Physique Colloque C6, C6-631 (1981).

11. J. Sapriel, J. C. Michel, J. C. Toledano, R. Vacher, J. Kervarec, and A. Regreny, Phys. Rev. B28, 2007 (1983).

12. J. E. Zucker, A. Pinczuk, D. S. Chemla, A. Gossard, and W. Wiegmann, Phys. Rev. Lett. 51, 1293 (1983).

13. B. Jusserand, D. Paquet, J. Kervarec, and A. Regreny, in Proceedings of the International Conference on the Dynamics of Interfaces, Lille, France, 1983 (to be published).

14. S. K. Yip and Y. C. Chang, unpublished work.

15. K. Kunc and R. M. Martin, in Proc. 16th Int. Conf. on the Physics of Semicond., ed. by M. Averous (North Holland, Amsterdam, 1983), p. 511.

16 S. M. Rytov, Sov. Phys. Acous. 2, 67 (1956).

17. O. K. Kim and W. G. Spitzer, J. Appl. Phys. 50, 4362 (1979).

18. S. M. Rytov, Sov. Phys. JETP 2, 466 (1956).

19. W. Hayes and R. Loudon, Scattering of Light by Crystals (John Wiley and Sons, New York, 1978).

20. S.-Y. Ren and W. A. Harrison, Phys. Rev. B23, 762 (1981).

21. Landolt-Börnstein Tables, ed. O. Madelung (Springer-Verlag, Berlin, 1982), Group III, Vol. 17a.

22. R. M. Fleming, D. B. McWhan, A. C. Gossard, W. Wiegmann, and R. A. Logan, J. Appl. Phys. 51, 357 (1980).

23. G. Dolling and J. L. T. Waugh, in Lattice Dynamics, ed. by R. F. Wallis (Pergamon, 1965), p. 19.

24. Data taken by W. J. Bartels, Philips Research Laboratories, Eindhoven.

FIGURE CAPTIONS

1 Model used for linear chain calculations. AlAs layer thickness is $d_2 = n\varepsilon$.

2 Real and imaginary part of phonon wavevector q. Dashed lines: transverse modes. Solid lines: longitudinal modes. Parameters of model are fit to circled points.

3 Linear chain model calculation of phonon dispersion curves for longitudinal and transverse modes. Large zone: bulk GaAs and AlAs. Small zone: (5,4) superlattice. q given in Å^{-1}.

4 Frequency of interface-like optic modes versus AlAs layer thickness - d_1:GaAs layer, d_2:AlAs layer.

5 Raman spectrum of sample (42Å, 8Å:0.3); $\lambda_L = 5145\text{Å}$, T = 300K. Inset is Rytov model calculations showing q of folded LA peaks.

6 Samples (20Å, 12Å:1), (41Å, 8Å:1), (59Å, 20Å:0.3), and (41Å, 41Å:0.3); $\lambda_L = 5145\text{Å}$, T = 300K. Sharp peaks are folded LA phonons, 2TA is at 160 cm^{-1}.

7 Phonon dispersion near first folded LA gap for a (5,4) superlattice, capculated with linear chain model. Data points are folded peaks in sample (14Å, 12Å:1) at several laser wavelengths. q_z is in units of π/d.

8 Raman spectrum of sample (14Å, 12Å:1); $\lambda_L = 5145\text{Å}$, T = 300K, near first folded gap. Strong peaks are LA phonons, T indicates transverse phonons.

9 Composite plot of folded acoustic phonon frequencies vs. inverse period. Circles refer to samples with alloy barriers, squares to those with pure AlAs barriers. The two doublets at lower right are transverse modes. Shaded regions are bounded by folded AlAs and GaAs bulk sound waves $\omega = (2\pi m/d)v_s$.

10 Raman spectrum of sample (41Å, 41Å:0.3); λ_L = 5145Å, T = 300K. Inset is Rytov model calculation showing q of folded LA phonons and missing second order peaks.

11 Raman spectra of sample (85Å, 88Å:0.3) for two values of λ_L; (x,x) geometry, T = 300K. Inset is Rytov model calculation showing q of peaks in lower curve and missing modes. Upper resonant spectrum shows interference-type behavior.

12 X-ray diffraction spectrum of sample (85Å, 88Å:0.3) showing negligible second order satellite.

13 Raman spectra of folded LA phonons from sample (41Å, 8Å:1) annealed at 850K for 0, 1, 4, and 9 hrs; λ_L = 5145Å, T = 300K, (x,x) geometry.

14 Raman spectra near the band gap of sample (14Å, 12Å:); λ_L = 6328Å, T = 300K. Spikes above 100 cm^{-1} are Ne calibration lines.

15 Raman spectra of 3 samples showing disorder activated structure. From top to bottom the samples are (11Å, 10Å:1), (38Å:0.25, 13Å:1), and (14Å:0.5, 14Å:1) λ_L = 5145Å, T = 300K.

16 Raman spectra of sample (12.5Å, 37.5Å:1) showing disorder activated structure at two temperatures; λ_L = 5145Å.

17 Optical phonon Raman spectra of 4 samples with AlAs barriers. Strong peaks are in (x,y) geometry, weak curve is (x,x). From top to bottom the samples are: (14Å, 12Å:1); (20Å, 12Å:1); (27Å, 11Å:1); (41Å, 8Å:1).

18 Raman spectrum near GaAs-like optic branch of sample (20Å, 12Å:1). λ_L = 6764Å, T = 180K.

19 Resonance behavior of peaks labeled in Fig. 18. A refers to lowest folded acoustic phonon. Band gap was tuned through λ_L by varying temperature. Intensity not corrected for absorption. ω_o is 300K luminescence peak.

20 Composite plot of optical phonon frequencies squared vs. inverse square layer period. d_1 = GaAs layer thickness, d_2 = AlAs. Straight lines are $\omega^2 = \omega_L^2 - v_s^2(\ell\pi/d_{1,2})^2$ for ℓ = 1,2, or 3. Unless specified, peaks appear in (x,y) geometry.

21 Raman spectra of GaAs-like optic phonons from sample (41Å, 8Å:1) annealed at 850K for 0, 1, 4, 16 hours; λ_L = 5145Å, T = 300K, (x,y) geometry.

22 Same as Fig. 21 for AlAs-like optic region.

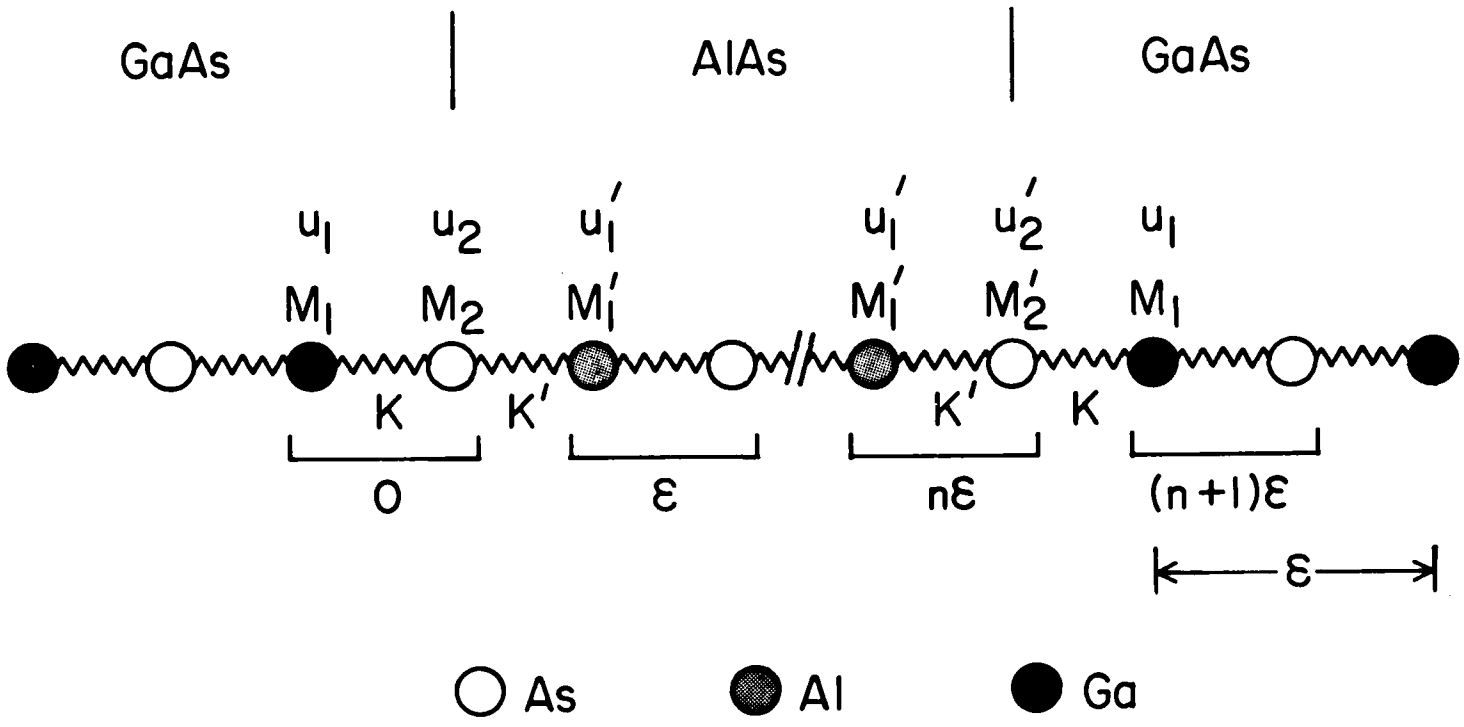
GaAs
AlAs
GaAs
u_1
u_2
u_1'
u_1'
u_2'
u_1
M_1
M_2
M_1'
M_1'
M_2'
M_1
K
K′
K′
K
0
ε
nε
(n+1)ε
ε
As
Al
Ga

Fig. 1.

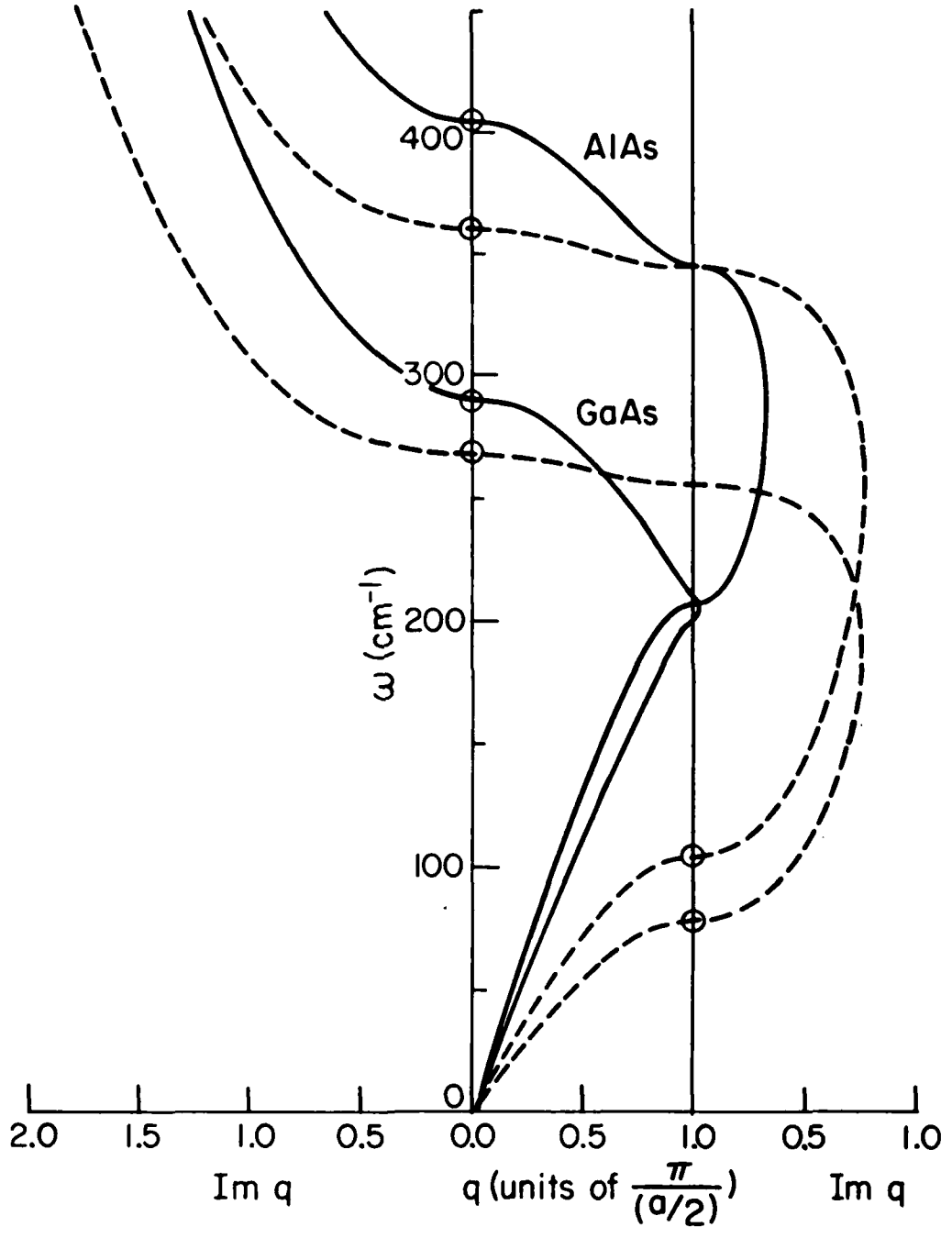
AlAs
GaAs
400
300
200
100
0
ω (cm⁻¹)
2.0
1.5
1.0
0.5
0.0
0.5
1.0
0.5
1.0
Im q
q (units of π/(a/2))
Im q

Fig. 2.

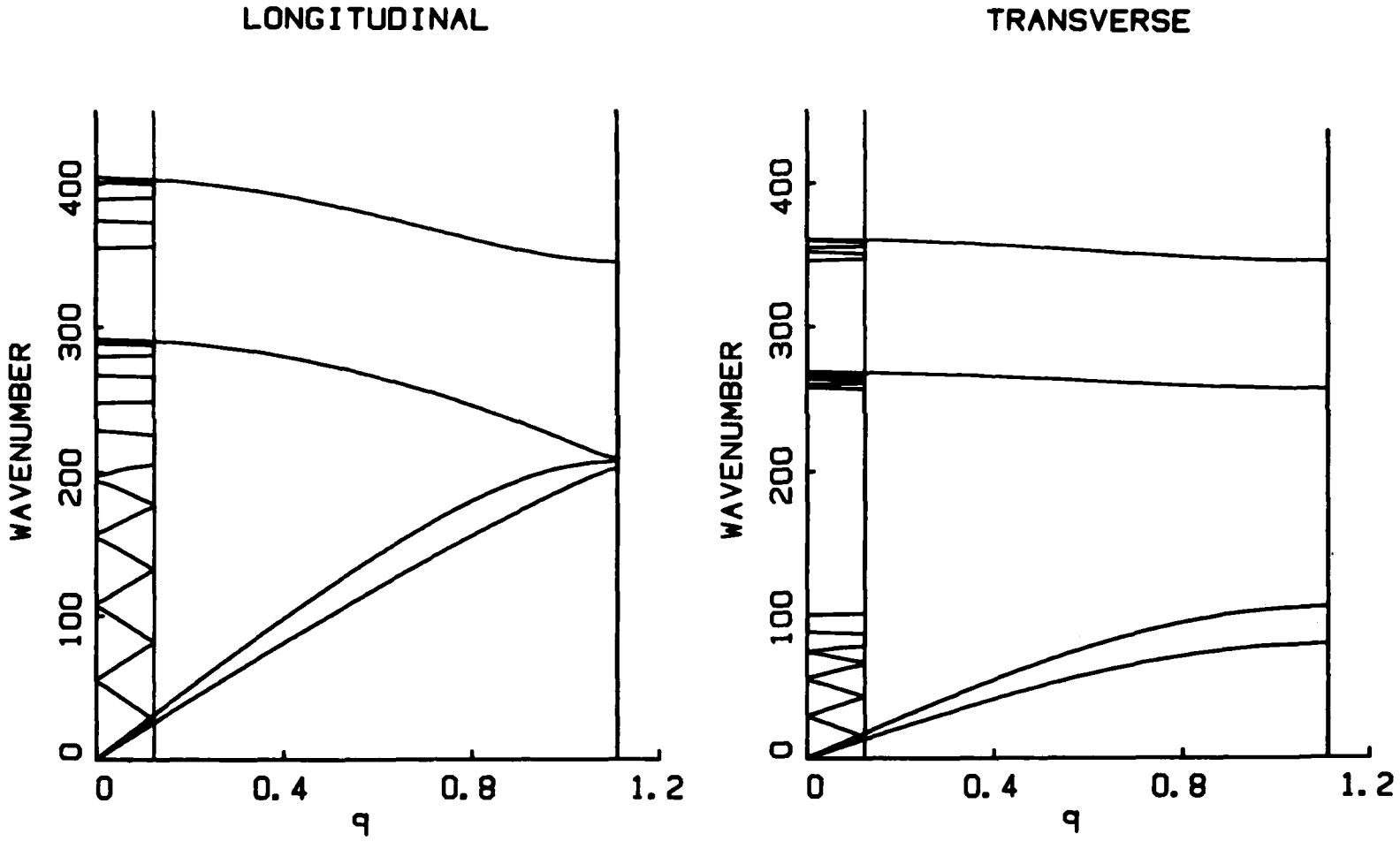
LONGITUDINAL
TRANSVERSE
WAVENUMBER
0
100
200
300
400
0
0.4
0.8
1.2
q

Fig. 3.

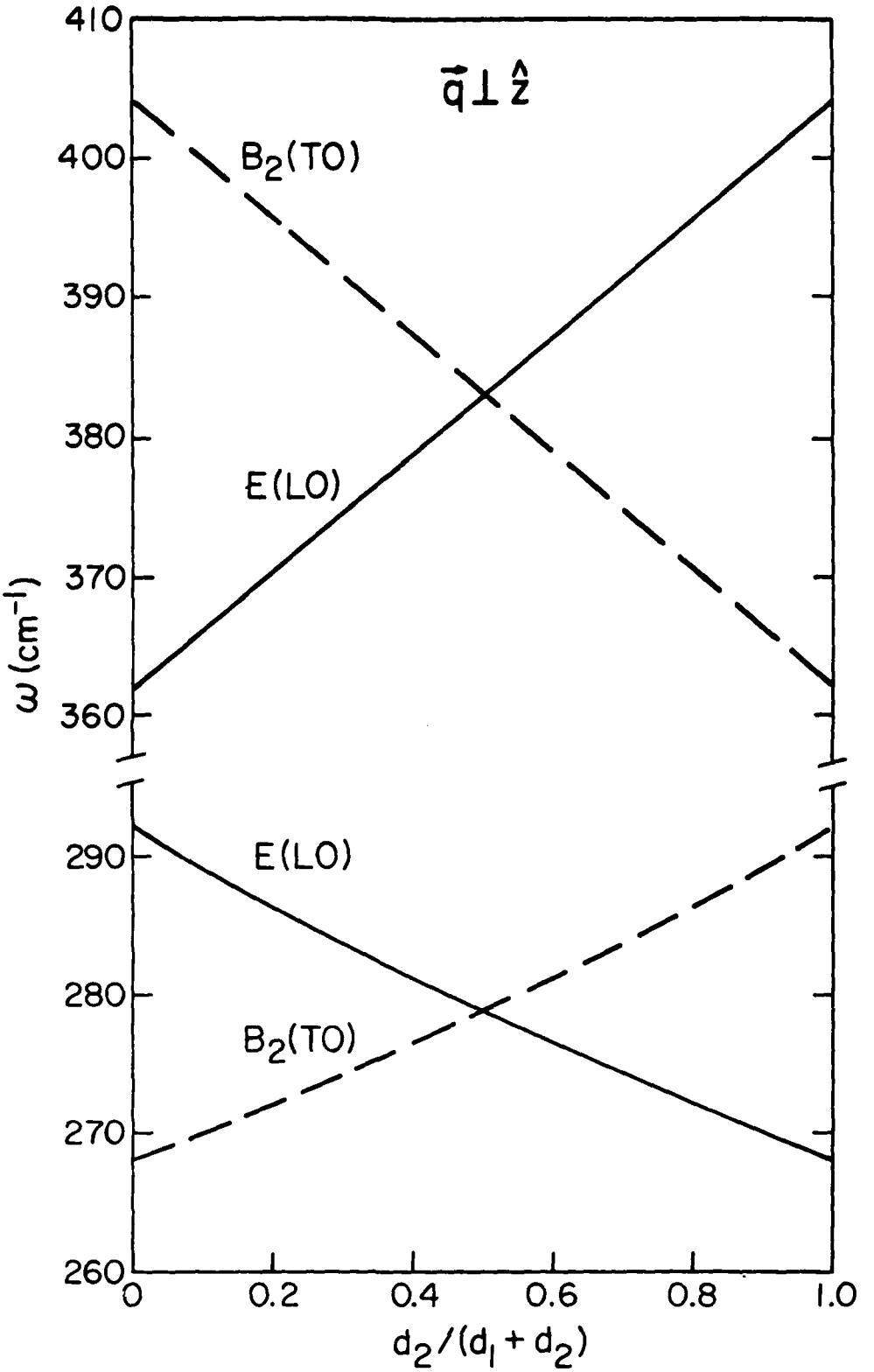
410
400
390
380
370
360
290
280
270
260
$\vec{q} \perp \hat{z}$
B_2(TO)
E(LO)
E(LO)
B_2(TO)
ω (cm^{-1})
0
0.2
0.4
0.6
0.8
1.0
$d_2/(d_1 + d_2)$

Fig. 4.

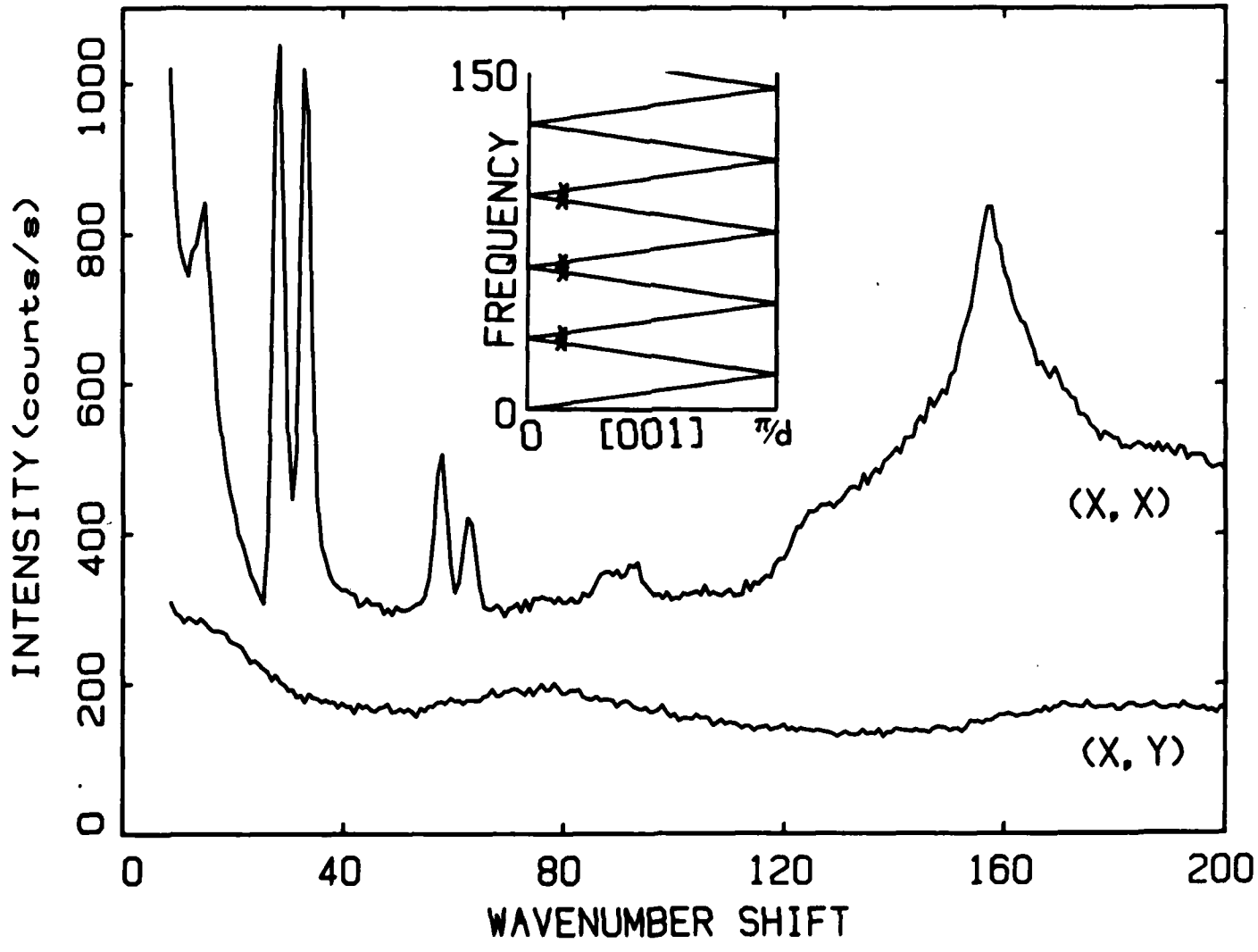
INTENSITY (counts/s)
0
200
400
600
800
1000
0
40
80
120
160
200
WAVENUMBER SHIFT
(X, X)
(X, Y)
150
FREQUENCY
0
0
[001]
π/d

Fig. 5.

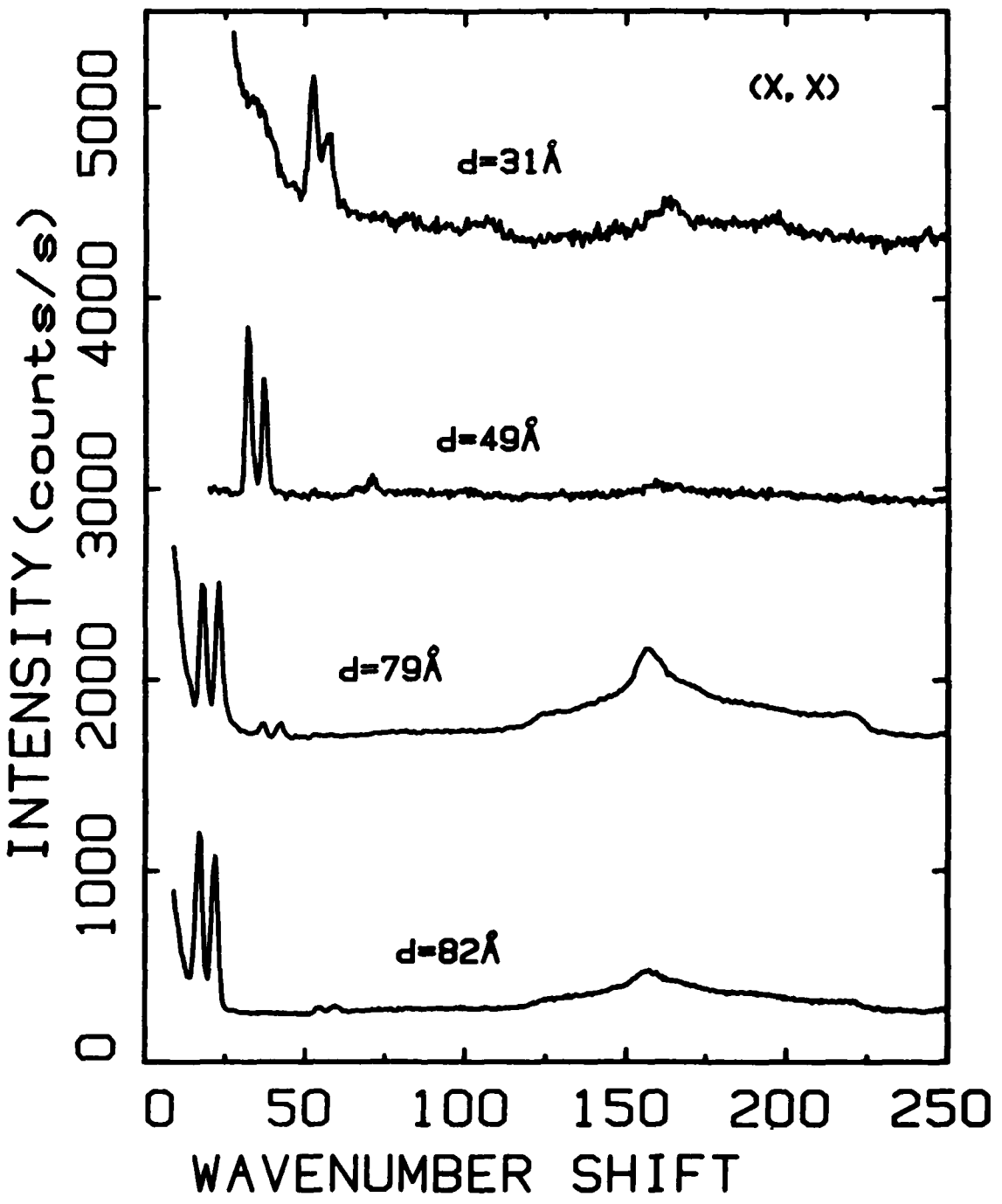
(X, X)
d=31Å
d=49Å
d=79Å
d=82Å
INTENSITY(counts/s)
0
1000
2000
3000
4000
5000
0
50
100
150
200
250
WAVENUMBER SHIFT

Fig. 6.

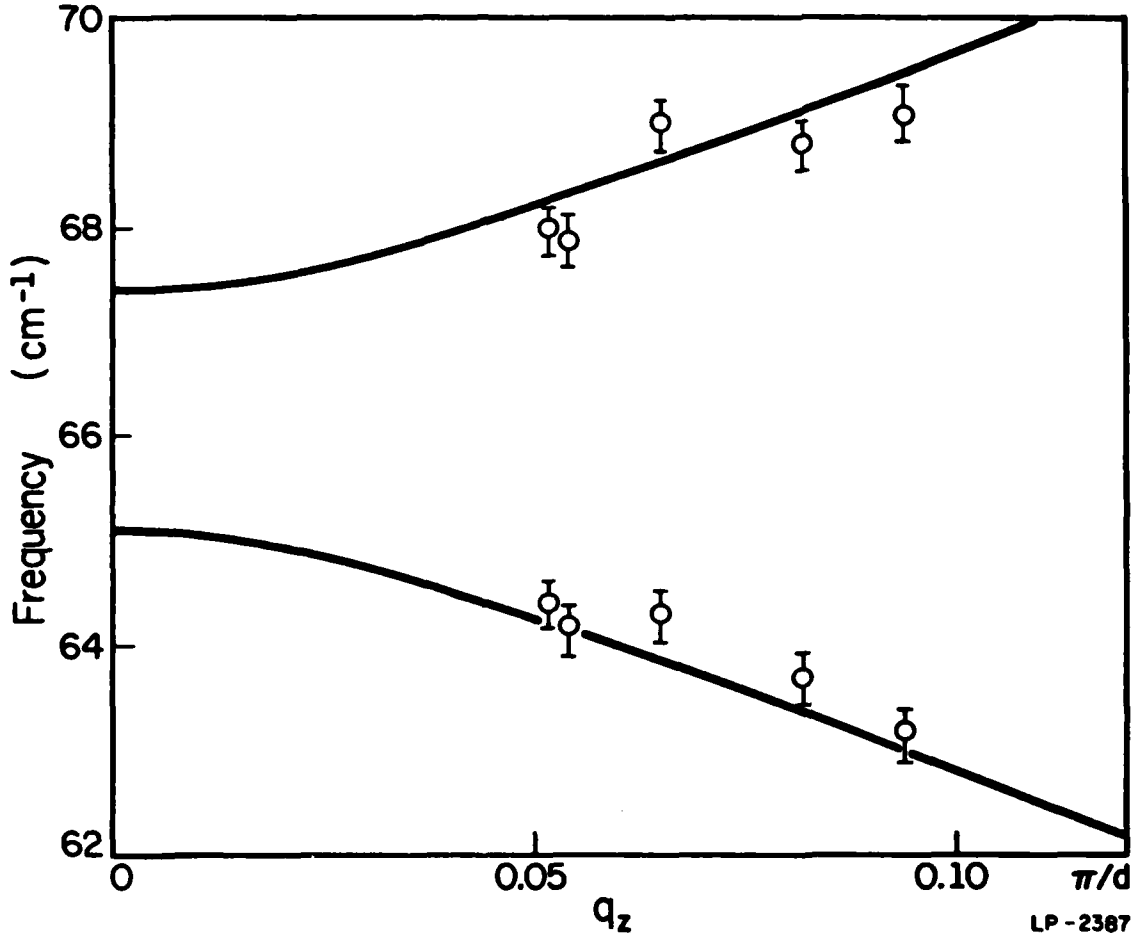

Fig. 7.

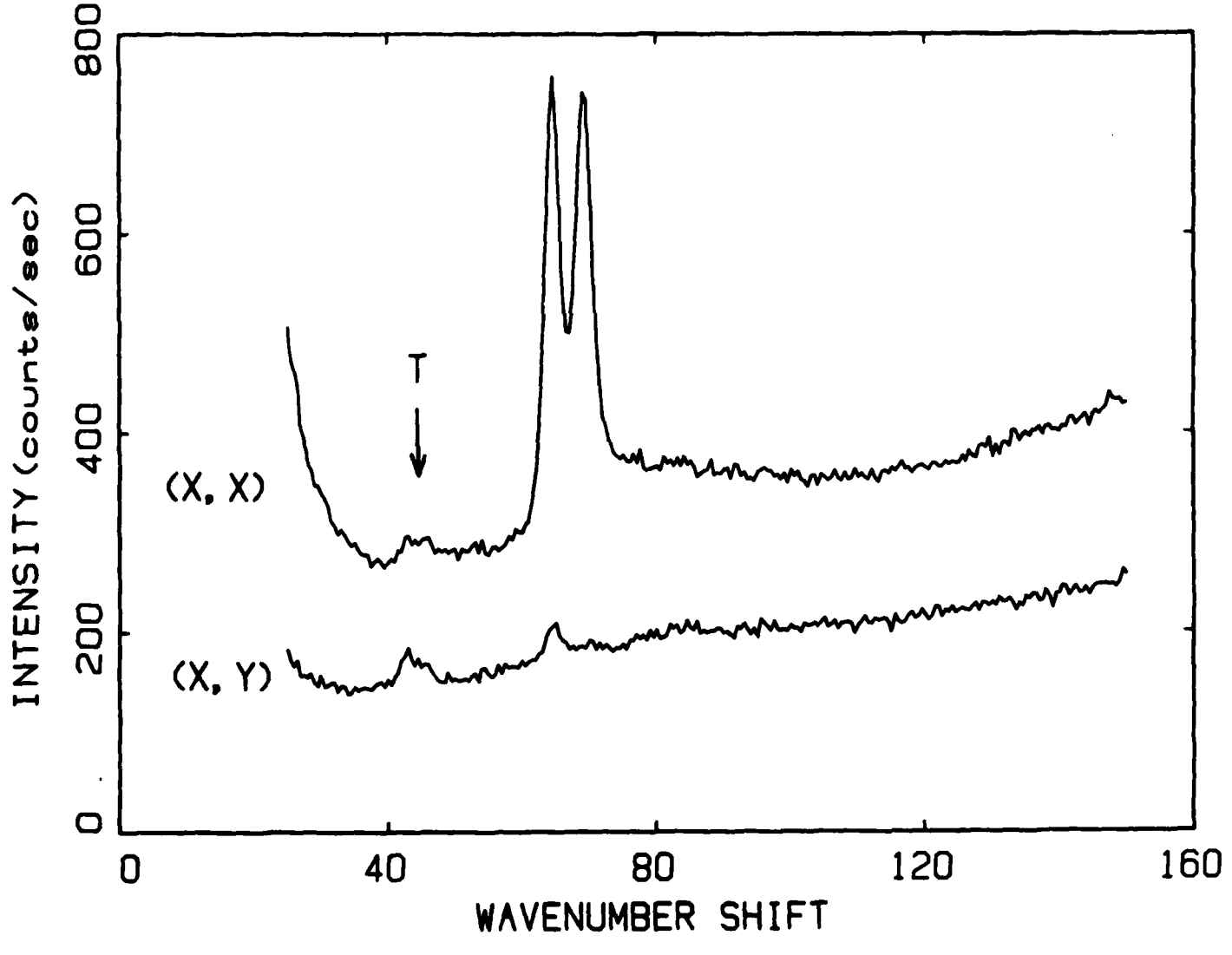
INTENSITY (counts/sec)
800
600
400
200
0
T
(X, X)
(X, Y)
0
40
80
120
160
WAVENUMBER SHIFT

Fig. 8.

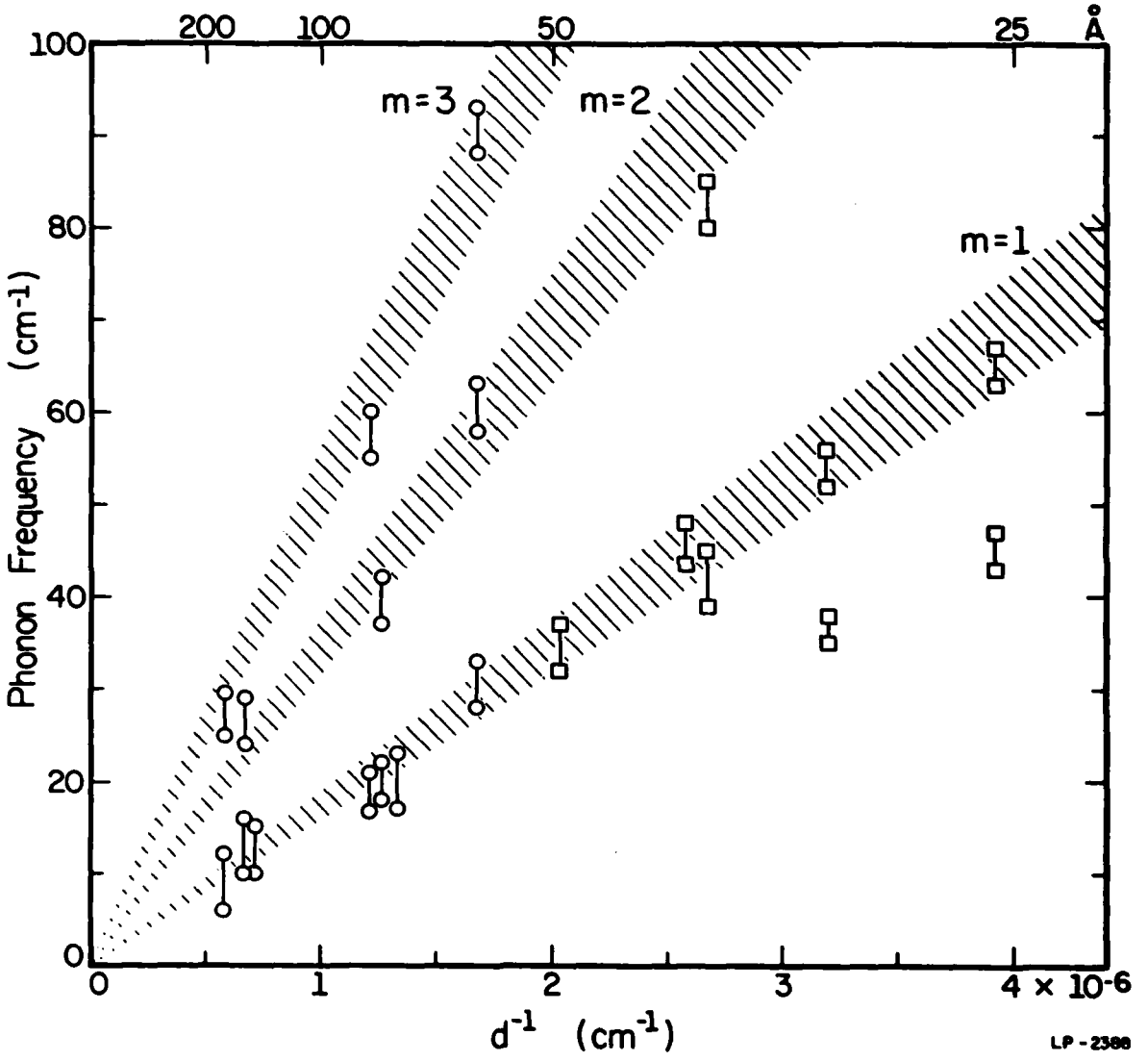
200
100
50
25
Å
100
80
60
40
20
0
m=3
m=2
m=1
Phonon Frequency (cm-1)
0
1
2
3
4 x 10-6
d-1 (cm-1)
LP-2388

Fig. 9.

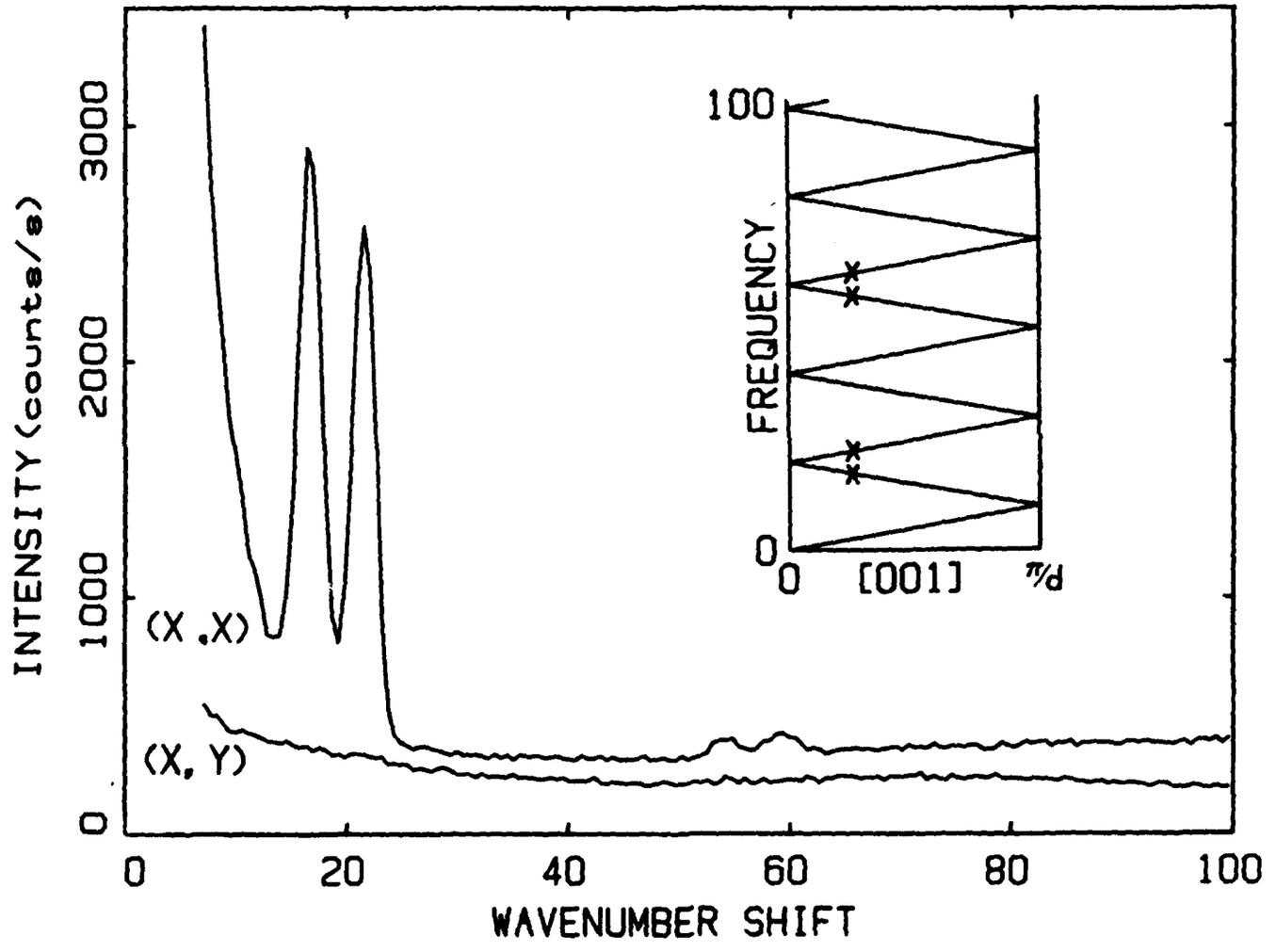
INTENSITY (counts/s)
3000
2000
1000
0
(X ,X)
(X, Y)
0
20
40
60
80
100
WAVENUMBER SHIFT
100
FREQUENCY
0
0
[001]
π/d

Fig. 10.

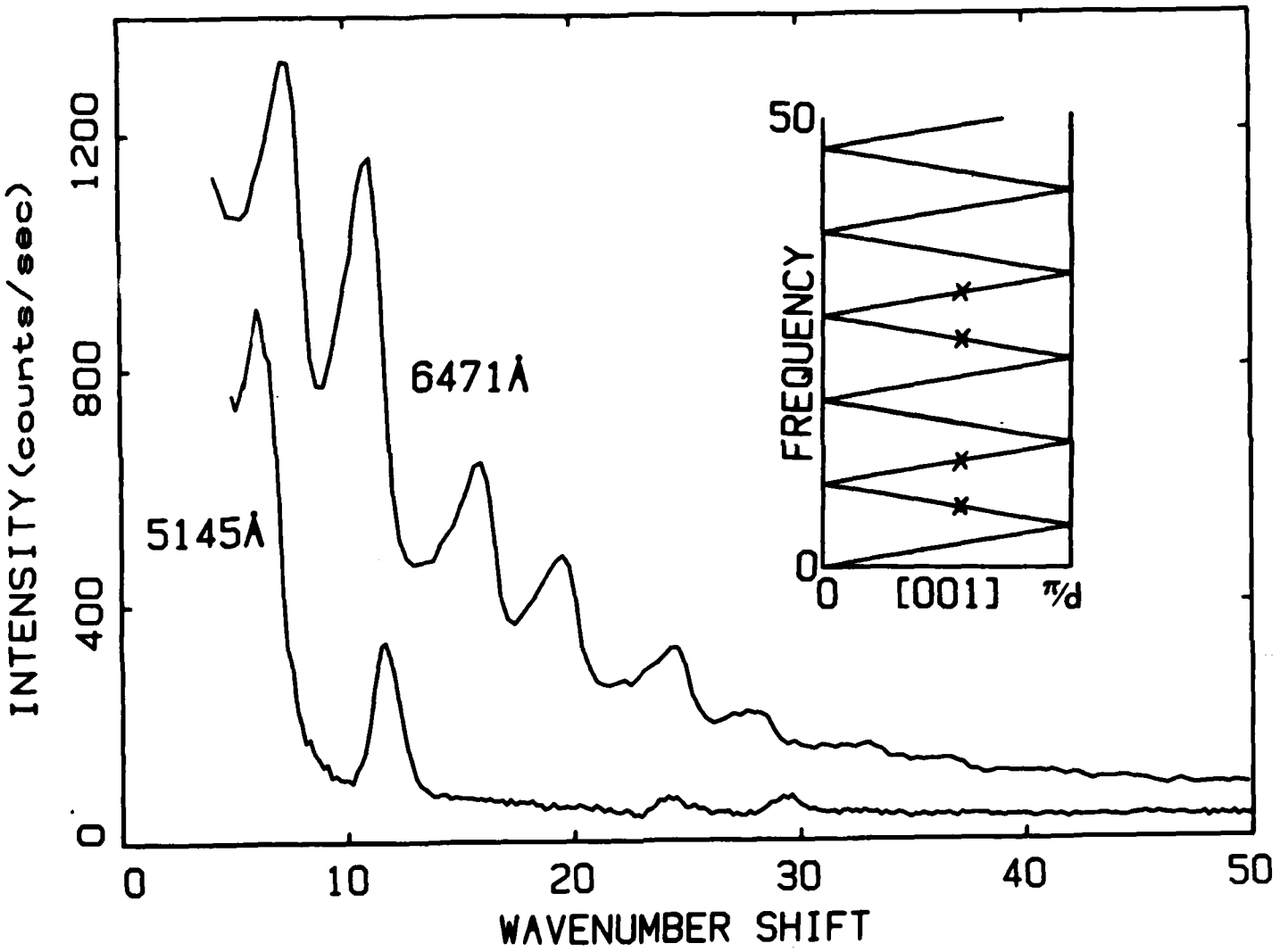
INTENSITY (counts/sec)
0
400
800
1200
6471Å
5145Å
0
10
20
30
40
50
WAVENUMBER SHIFT
FREQUENCY
50
0
0
[001]
π/d

Fig. 11.

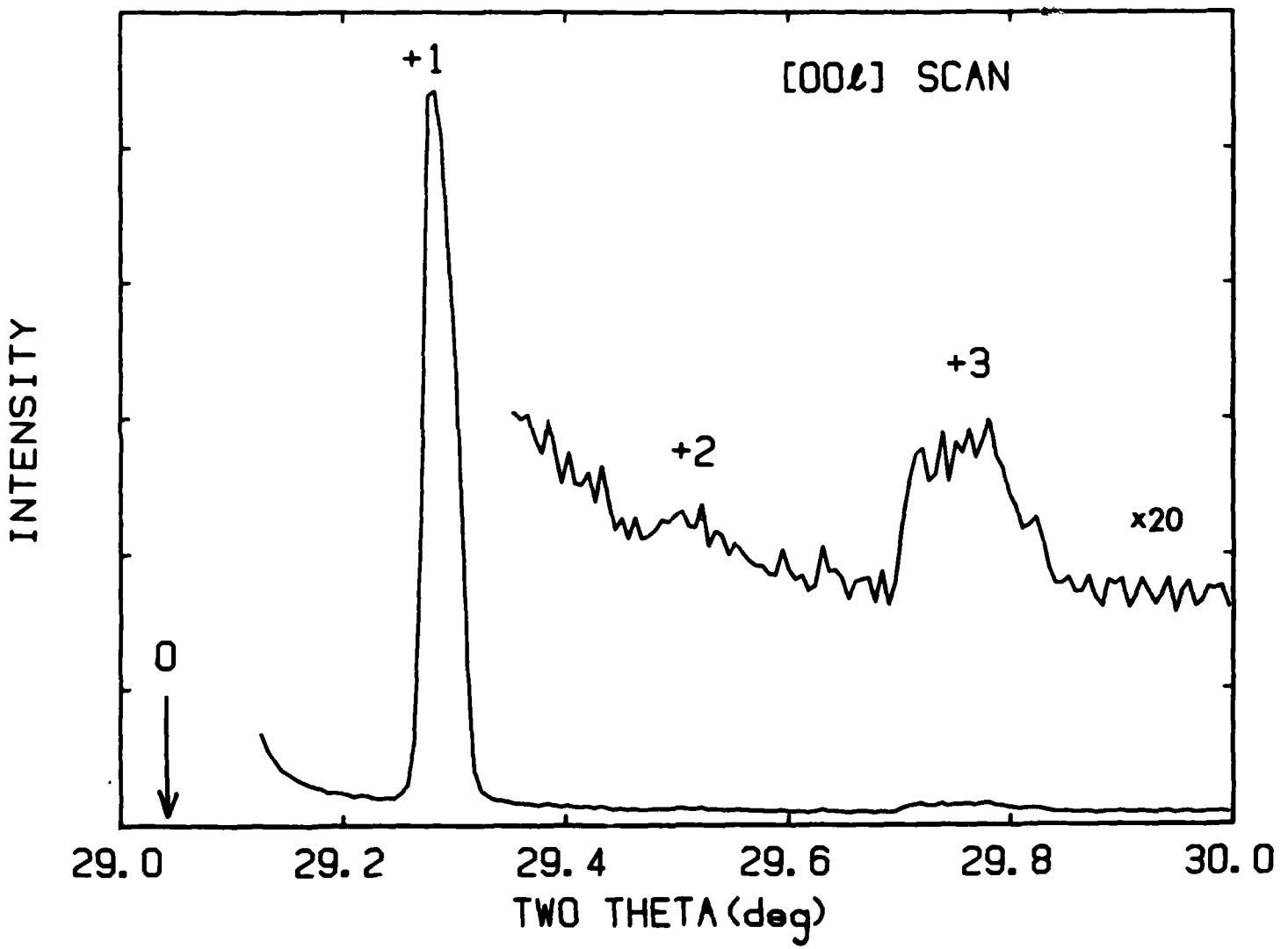
[00ℓ] SCAN
+1
+2
+3
x20
0
INTENSITY
29.0
29.2
29.4
29.6
29.8
30.0
TWO THETA (deg)

Fig. 12.

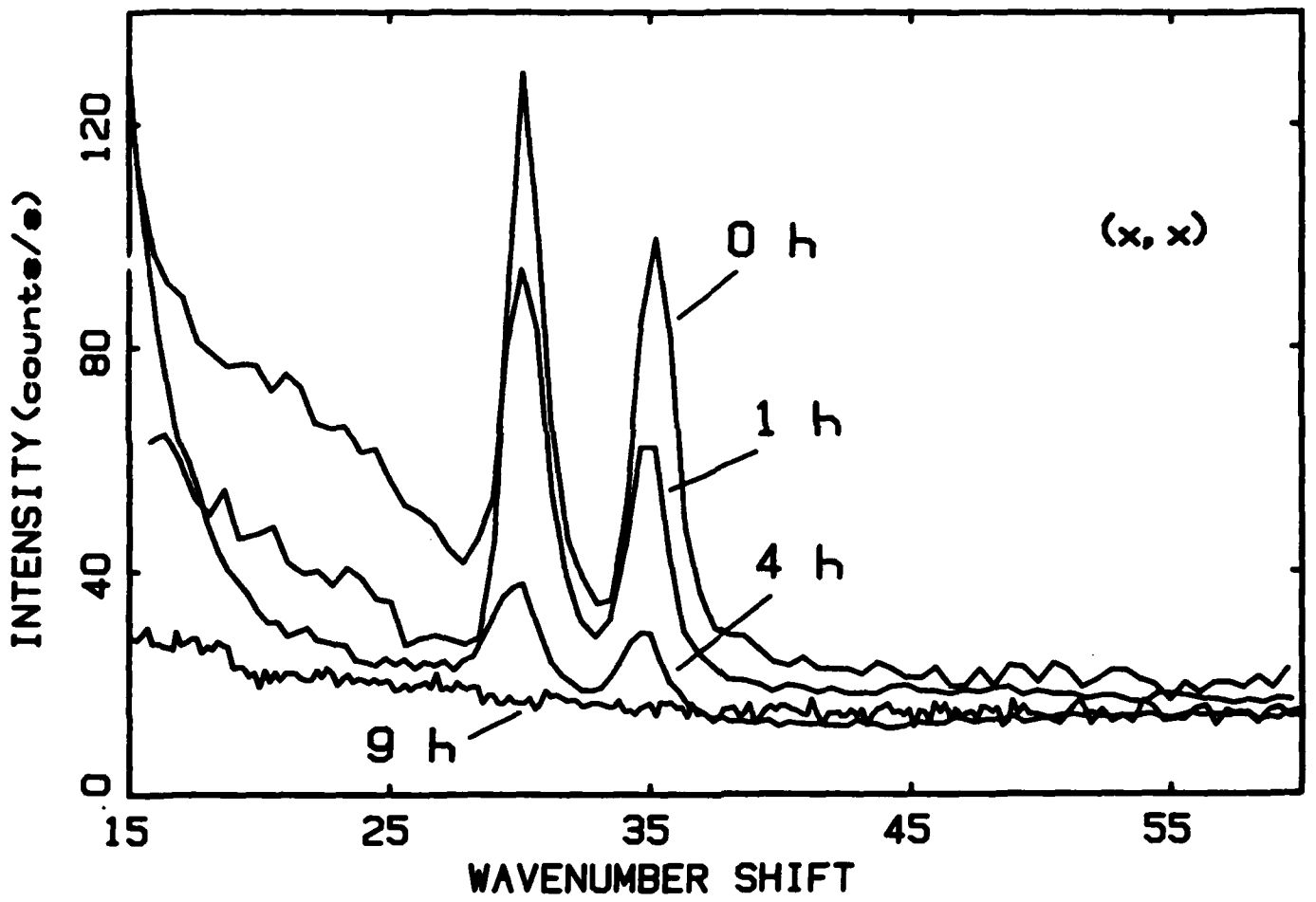
INTENSITY (counts/s)
0
40
80
120
15
25
35
45
55
WAVENUMBER SHIFT
0 h
1 h
4 h
9 h
(x, x)

Fig. 13.

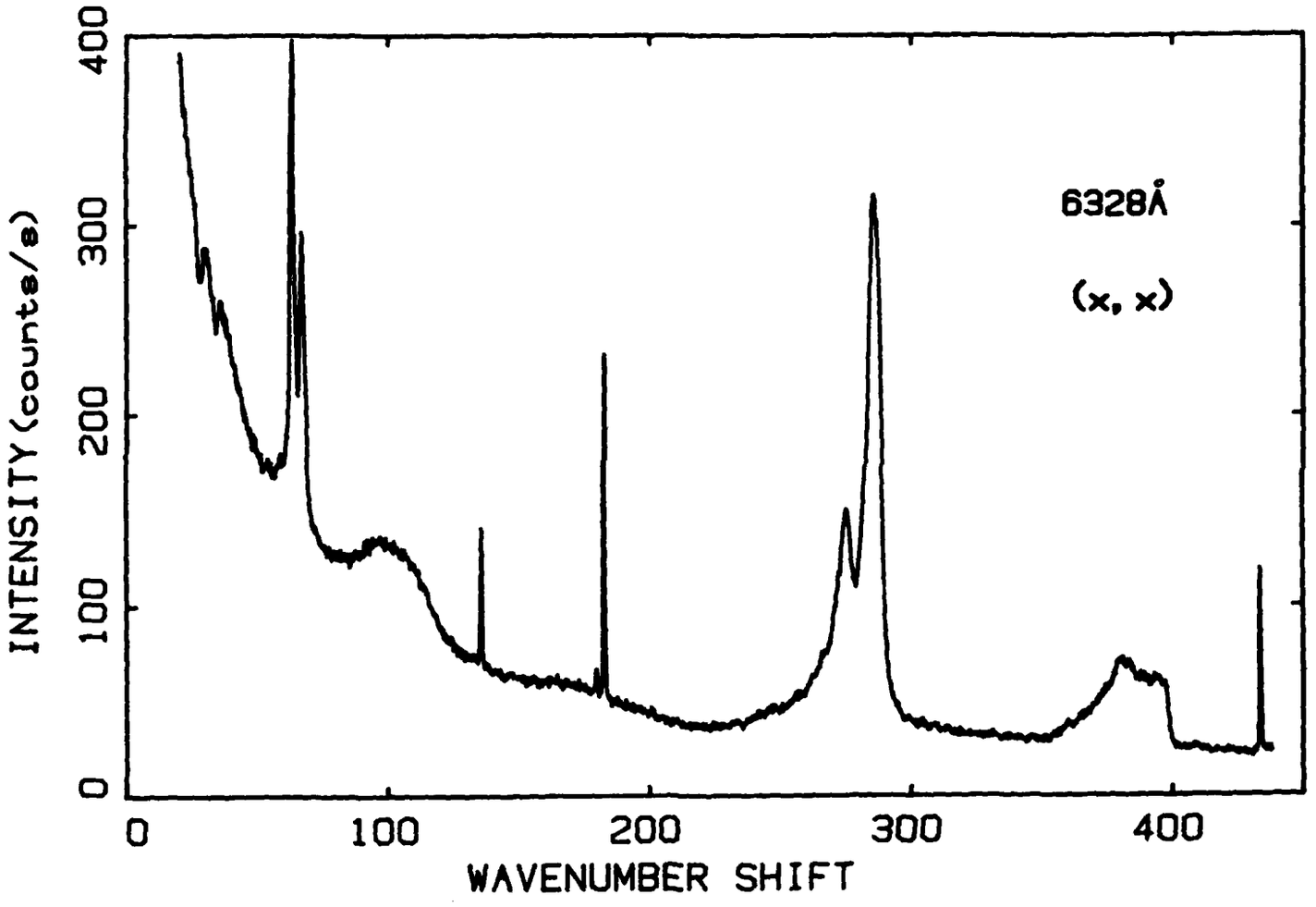
INTENSITY (counts/s)
0
100
200
300
400
WAVENUMBER SHIFT
6328Å
(x, x)

Fig. 14.

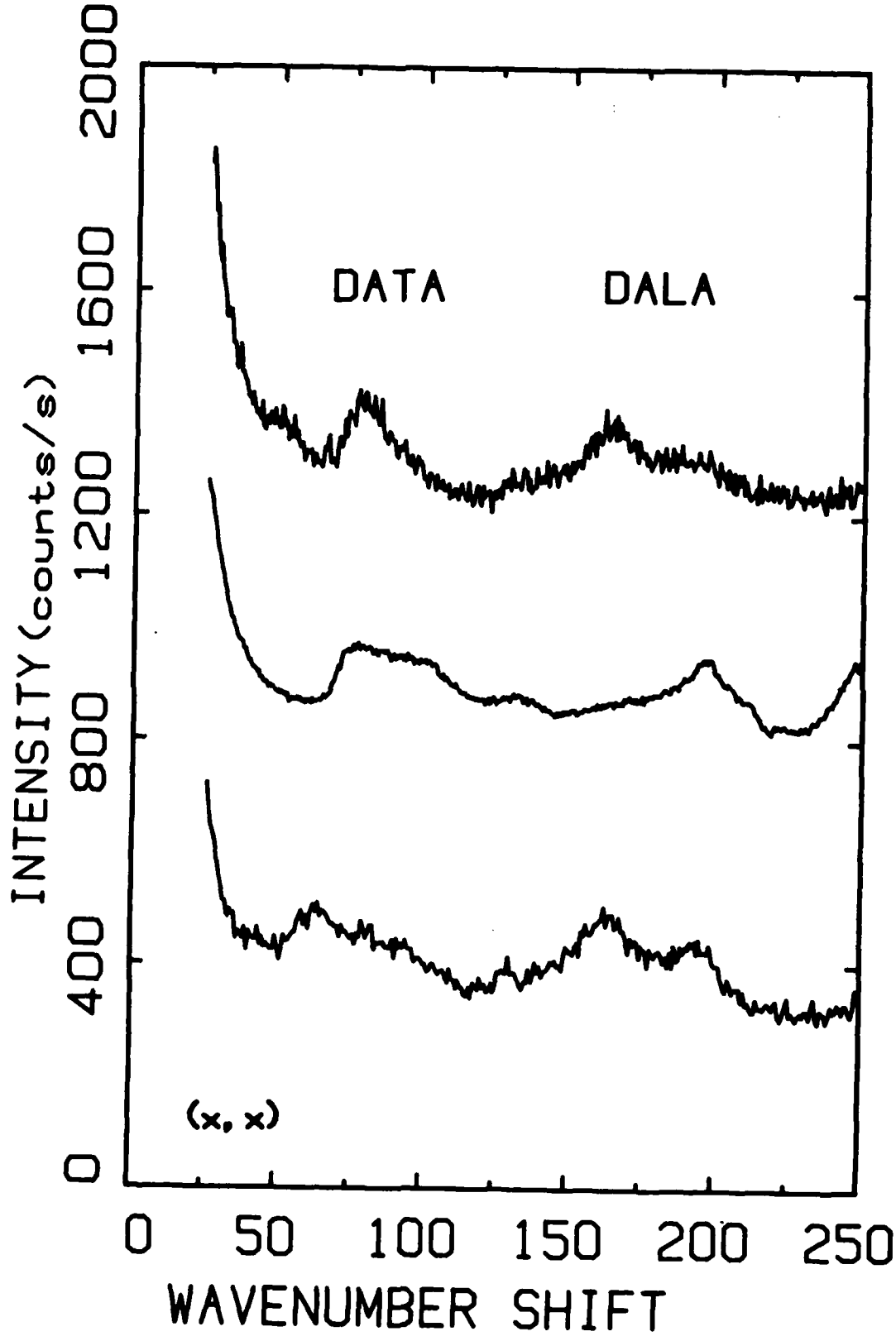
DATA
DALA
INTENSITY (counts/s)
0
400
800
1200
1600
2000
(x, x)
0
50
100
150
200
250
WAVENUMBER SHIFT

Fig. 15.

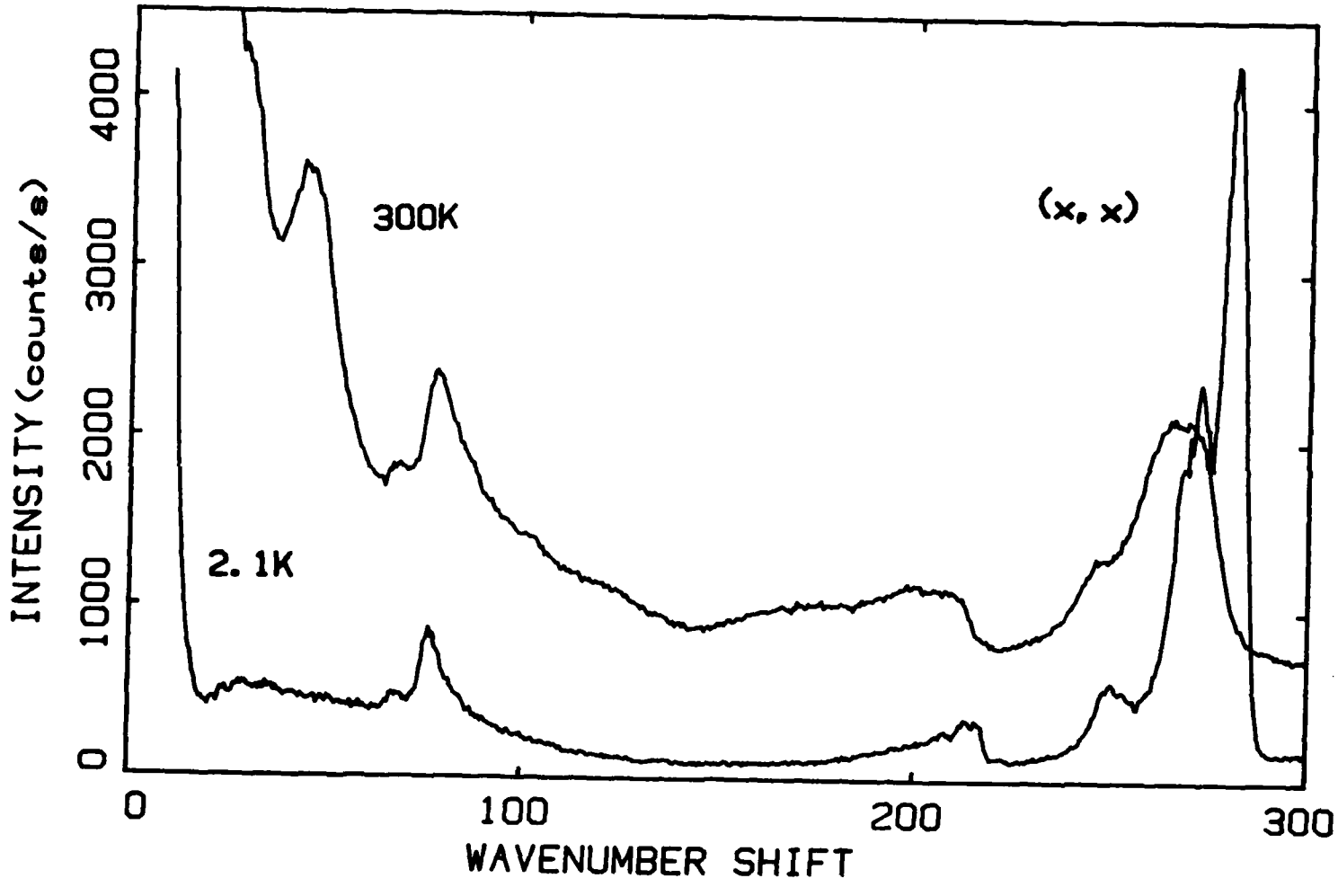
INTENSITY (counts/s)
0
1000
2000
3000
4000
300K
2.1K
(x, x)
0
100
200
300
WAVENUMBER SHIFT

Fig. 16.

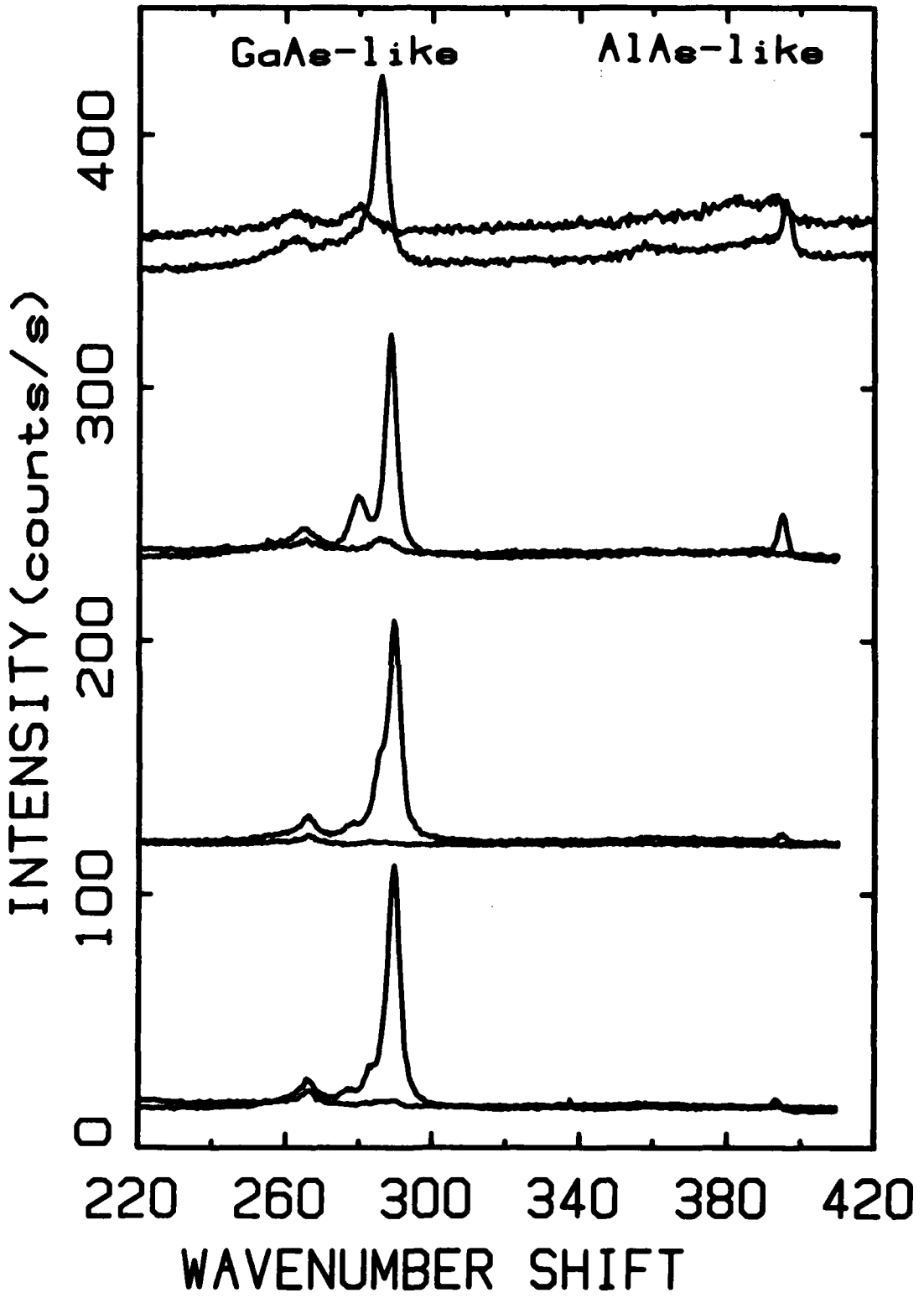
GaAs-like
AlAs-like
INTENSITY (counts/s)
400
300
200
100
0
220
260
300
340
380
420
WAVENUMBER SHIFT

Fig. 17.

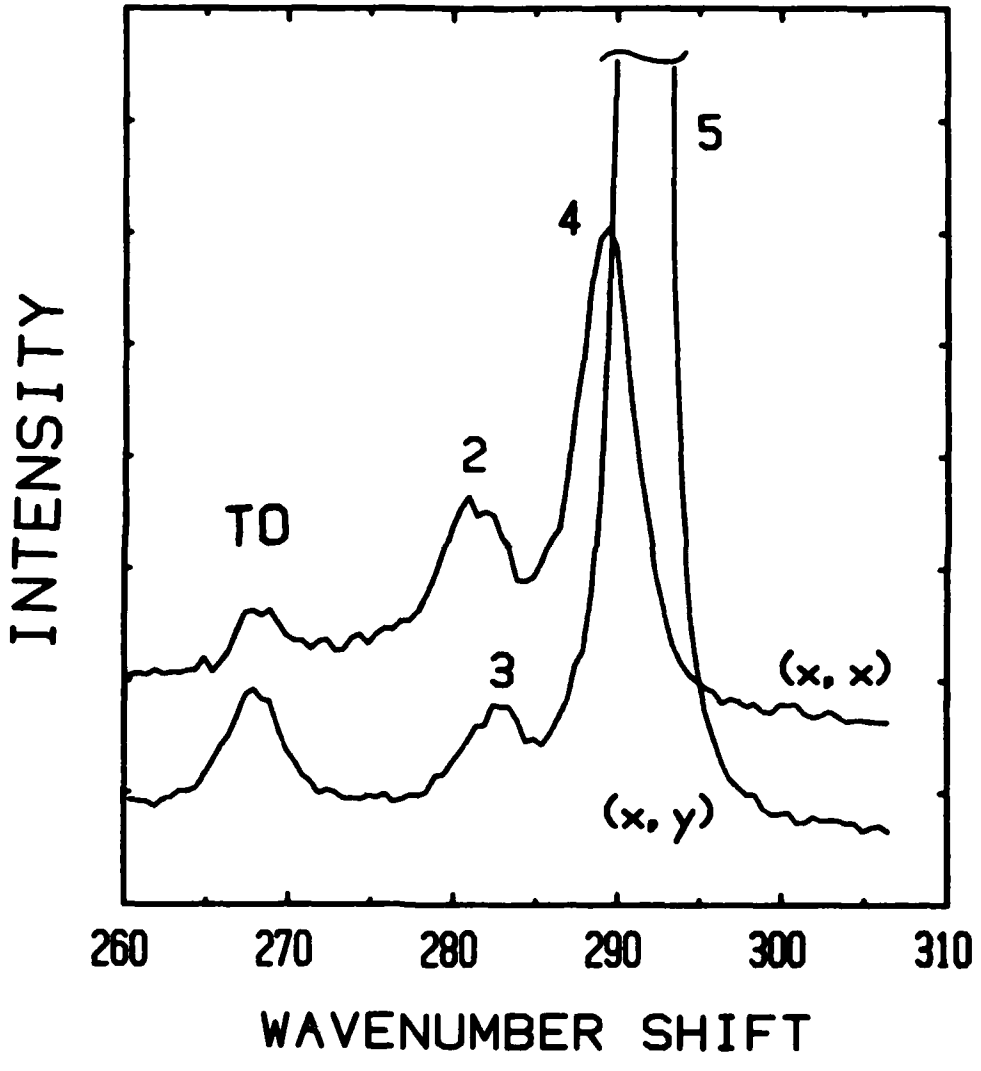
INTENSITY
TO
2
3
4
5
(x, x)
(x, y)
260
270
280
290
300
310
WAVENUMBER SHIFT

Fig. 18.

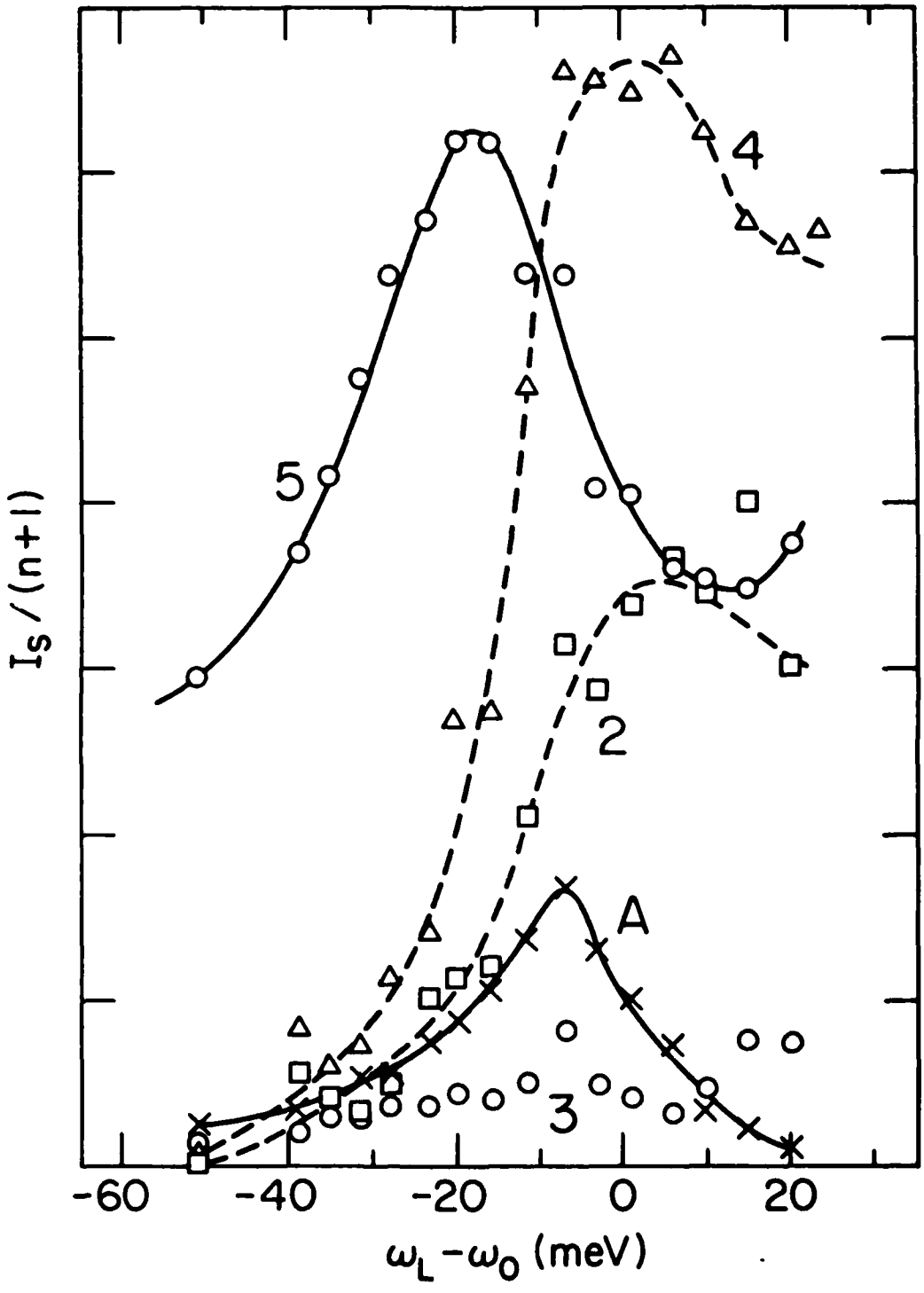

Fig. 19.

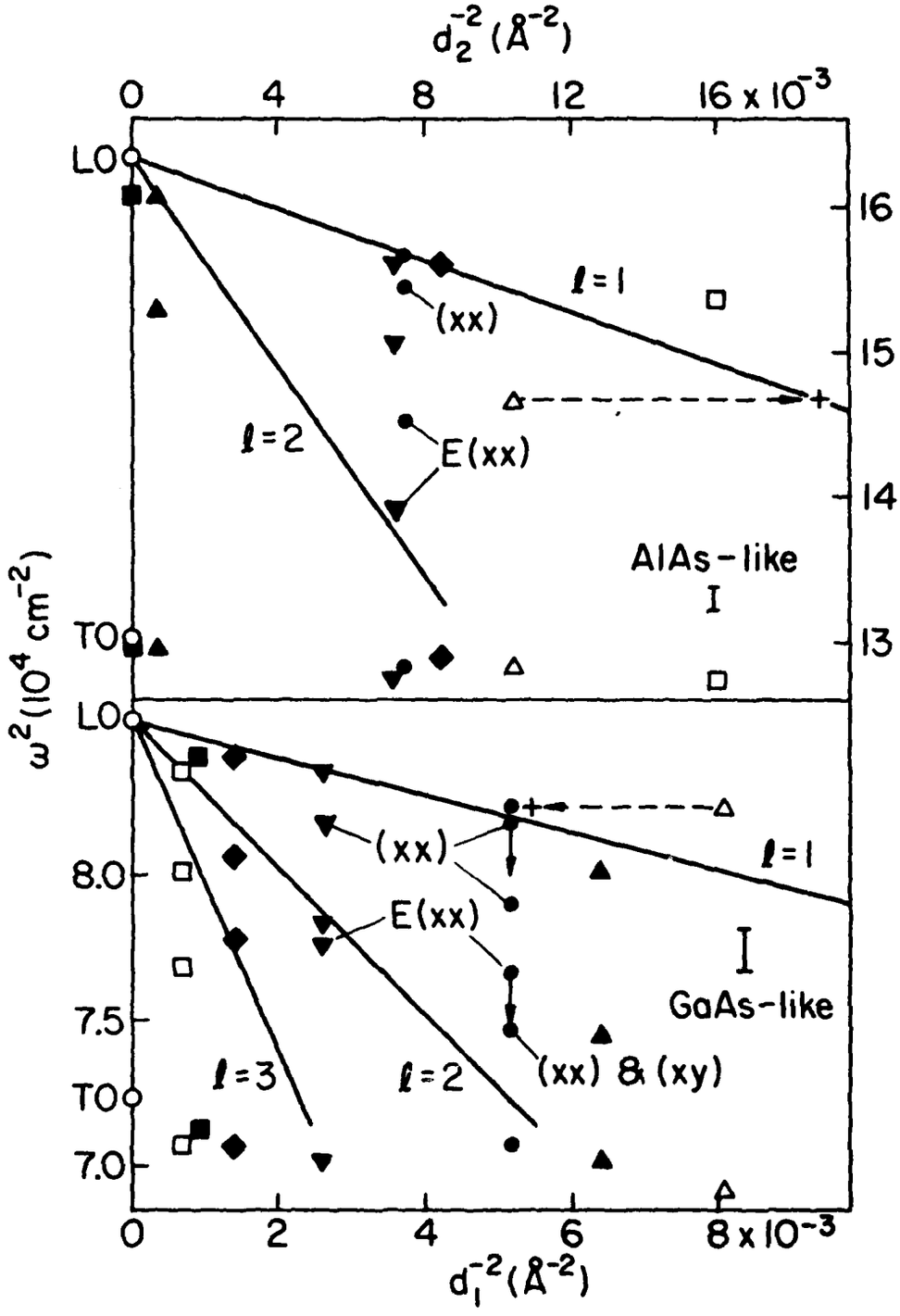
d_2^{-2} (Å^{-2})
0
4
8
12
16 x 10^{-3}
LO
TO
16
15
14
13
ℓ=1
(xx)
ℓ=2
E(xx)
AlAs-like
I
ω^2(10^4 cm^{-2})
LO
8.0
7.5
TO
7.0
(xx)
ℓ=1
E(xx)
I
GaAs-like
ℓ=3
ℓ=2
(xx) & (xy)
0
2
4
6
8 x 10^{-3}
d_1^{-2} (Å^{-2})

Fig. 20.

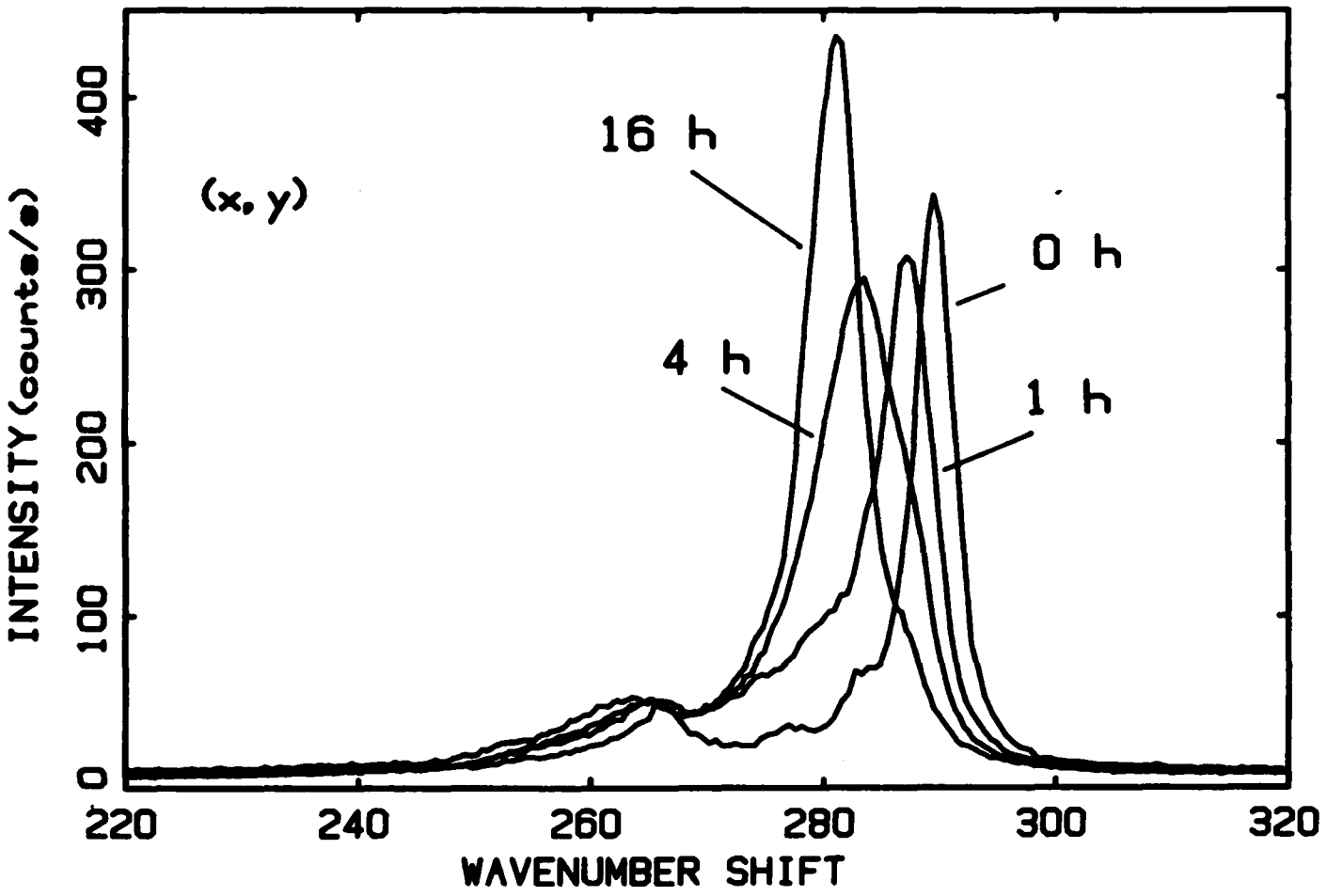
16 h
(x, y)
0 h
4 h
1 h
INTENSITY (counts/s)
0
100
200
300
400
220
240
260
280
300
320
WAVENUMBER SHIFT

Fig. 21.

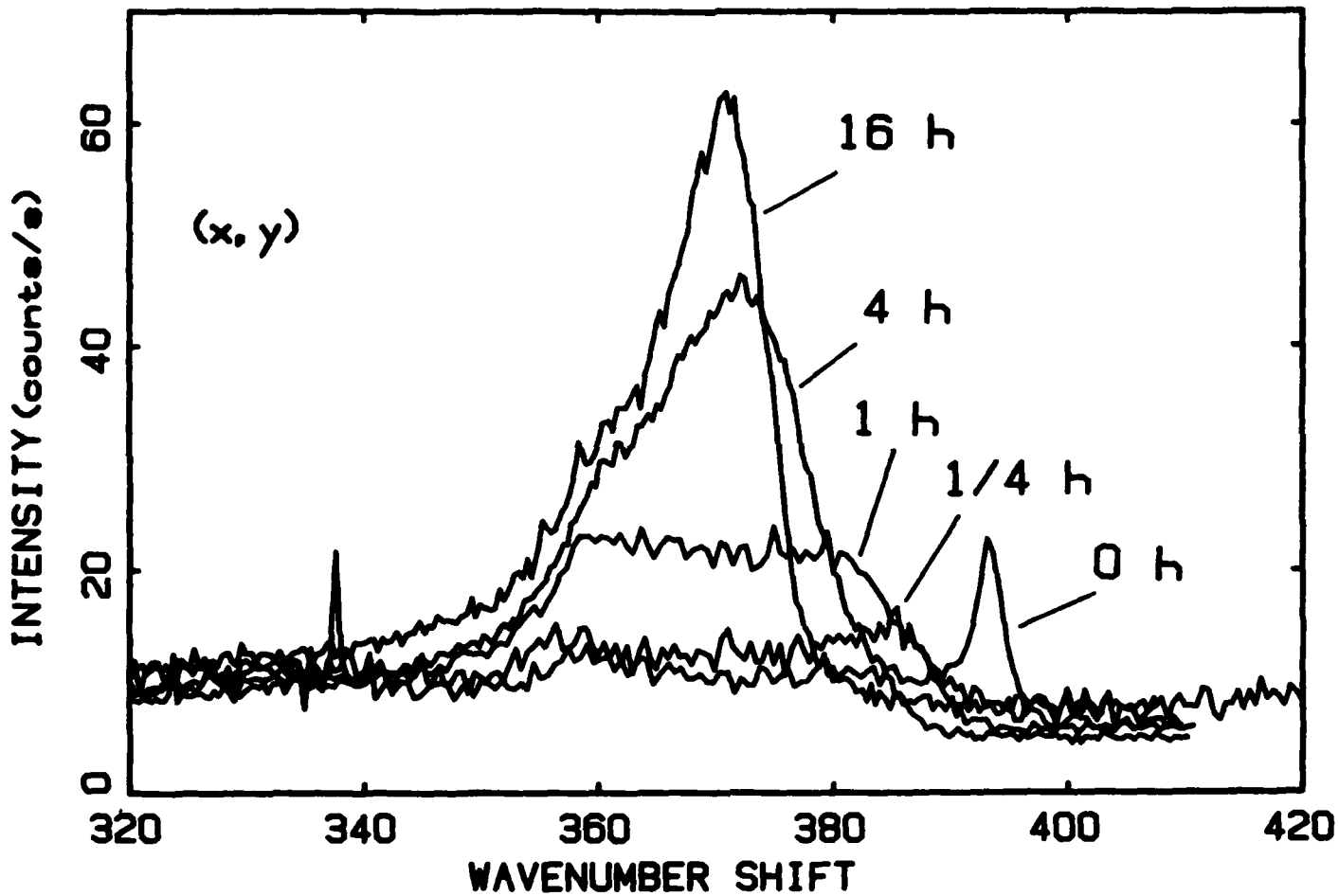
16 h
4 h
1 h
1/4 h
0 h
(x, y)
INTENSITY (counts/s)
0
20
40
60
320
340
360
380
400
420
WAVENUMBER SHIFT

Fig. 22.

Solid State Communications, Vol.45,No.10, pp.895-898, 1983. 0038-1098/83/100895-04$03.00/0
Printed in Great Britain. Pergamon Press Ltd.

RAMAN SCATTERING FROM CRYSTALLINE AND AMORPHOUS $(GaSb)_{1-x}Ge_x$ SEMICONDUCTING FILMS

T. N. Krabach
Department of Physics, University of Illinois
Urbana, Illinois 61801 USA

N. Wada*
Materials Research Laboratory and Coordinated Science Laboratory, University of Illinois
Urbana, Illinois 61801 USA

M. V. Klein
Department of Physics, Materials Research Laboratory
and Coordinated Science Laboratory, University of Illinois
Urbana, Illinois 61801 USA

K. C. Cadien**
Department of Metallurgy and Coordinated Science Laboratory, University of Illinois
Urbana, Illinois 61801 USA

and

J. E. Greene
Materials Research Laboratory, Department of Metallurgy
and Coordinated Science Laboratory, University of Illinois
Urbana, Illinois 61801 USA

(Received August 17, 1982 by R.H. Silsbee)

The first reported Raman scattering experiments have been performed on single crystal and amorphous films of the metastable alloy $(GaSb)_{1-x}Ge_x$ with compositions across the pseudobinary phase diagram. In crystalline films, the optical phonons exhibit a "one-two" type mode behavior. Broadening and softening of the Raman peaks with increasing alloy concentrations are attributed to a relaxation of q-vector selection rules due to substitutional disorder on both the cation and anion sublattices. Additionally, disorder induced scattering from the zone-edge acoustic phonons was observed. In amorphous alloy films, the reduced Raman spectra were compared to the one-phonon densities of states of the end-member crystals. The resulting apparent lack of polarization dependence indicated that the amorphous films were of the random network type.

Semiconducting alloys have been extensively studied, not only because of their practical device applications, but because of fundamental interest in disordered systems. In particular, the lattice dynamics of mixed crystal and amorphous systems have been of great interest. Raman and infrared spectroscopies have been employed to investigate the behavior of long-wavelength optical phonons in mixed crystals as a function of composition. The observed behavior generally falls into one of two classes.[1] The spectra of mixed crystals with one-mode behavior display a single set of optical modes; as the composition is varied the strength of these modes remains approximately constant, while their energy shifts continuously from the optical mode energy of one end-member component to that of the other component. This pattern is typically found in I-VII materials. Mixed crystals displaying a two-mode behavior possess two sets of optical modes occurring close to those of each component with the strength of each mode dependent on the concentration of the corresponding component. Many of the III-V ternary alloys exhibit this two-mode behavior. However, several semiconductor alloys present more complex patterns. Ternary alloys such as $InAs_{1-x}Sb_x$[2] and $Ga_{1-x}In_xSb$[3] are found to display an intermediate behavior with two sets of optic modes observed over part of the composition range, with only one mode seen over the remaining range of compositions ("one-two" mode behavior). The alloy system $Si_{1-x}Ge_x$ exhibits a three mode behavior;[4,5] because both constituents can substitute freely on the diamond lattice, Si-Si, Ge-Ge, and Si-Ge bonds are present, and the modes observed are attributed to this. Several theories have been advanced to predict and explain the long-wavelength mode behavior in mixed crystals.[6-9]

In this paper we report the first Raman results on a novel semiconducting alloy $(GaSb)_{1-x}$

* Present address: Schlumberger-Doll Research, Ridgefield, CT 06877
** Present address: Materials Research Laboratory, Duke University, Durham, NC 27706

Ge_x which has recently been grown in both crystalline[10,11] and amorphous[12] forms with concentrations ranging across the pseudobinary phase diagram. It should be noted that this mixed crystal differs in several ways from previously studied alloys. The single crystal alloys are metastable over most of the investigated concentration range. The pseudobinary phase diagram of this system[13] shows that the equilibrium solid solubilities of GaSb in Ge and Ge in GaSb are only 6.5 ± 0.5 and 2.0 ± 0.5 mole %, respectively. Another difference from ternary alloys is that substitutuional disorder exists on both sublattices of the zincblende or diamond structure. It is unique that the substituting species are not isovalent substitutions; Ge provides both acceptors and donors when it is an impurity in GaSb, since it occupies both cation and anion sites in the lattice, while GaSb impurities in Ge provide Ga acceptors and Sb donors.

All $(GaSb)_{1-x}Ge_x$ alloys were deposited using a multitarget radio-frequency sputtering system that has been described elsewhere.[14,15] The single crystal films were epitaxially grown on semi-insulating (100) GaAs substrates under excess antimony pressures at growth temperatures ranging from 470 to 485°C. The amorphous $(GaSb)_{1-x}Ge_x$ mixtures were grown on Corning 7059 glass substrates at 60°C with no antimony overpressures. In both cases, the average film thickness was 1.5 μm.

Film compositions were determined from the wavelength dispersive analyses in a JEOL electron microprobe with an accuracy of 0.5 at.%. The structural perfection of the crystalline films was confirmed with the use of x-ray diffractometry, Debye-Scherrer patterns, and electron channelling. X-ray diffraction spectra exhibited very sharp (400) peaks whose widths were limited by instrumental resolution. Electron channelling patterns, taken with a 10 μm aperture, were sharp and found to be invariant while scanning over the sample, demonstrating the homogeneity of the film. The film lattice constants obeyed Vegard's law, varying linearly with composition.[16] Post-annealing experiments showed that the single crystal metastable films exhibited good temporal and thermal stability. The transformation to the equilibrium two phase state was found to occur at temperatures ranging from 475 to 525°C, depending upon the alloy composition. From measurements of the exothermic heat of transformation as well as calculations of the total free energy change, the lifetime of the single phase metastable state at room temperature was estimated to be of the order of 10^{29} years. In the present Raman experiments, irradiation with a well focused one watt Ar^+ laser beam had no effect on sample integrity.

The Raman measurements were performed with the sample at room temperature and under vacuum to avoid spurious scattering from the air molecules. Light at a wavelength of 514.5 nm from an Ar^+ laser was incident perpendicular to the (100) surface of the sample with the scattered light collected in the true backscattering geometry. A double monochromator and conventional photon counting electronics were used. The laser power was one watt for the single crystal alloy films. However, in the amorphous films the power was limited to 20 mW in order to avoid spontaneous crystallization.[17]

Figure 1 shows the Raman spectra from six single alloy samples, pure Ge, and pure GaSb. These spectra were taken with the incident light polarized along the [010] crystal axis and the scattered light analyzed along the [001] axis.

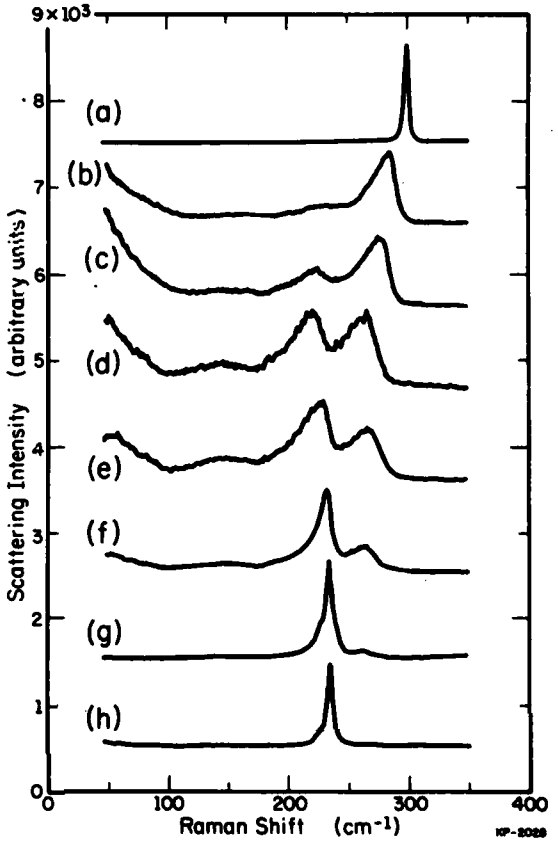

Fig. 1 Raman spectra from single crystals: a) Ge b) $(GaSb)_{0.27}Ge_{0.73}$ c) $(GaSb)_{0.44}Ge_{0.56}$ d) $(GaSb)_{0.66}Ge_{0.34}$ e) $(GaSb)_{0.76}Ge_{0.24}$ f) $(GaSb)_{0.86}Ge_{0.14}$ g) $(GaSb)_{0.94}Ge_{0.06}$ h) GaSb. All spectra were taken in the z(xy)z configuration with a 514.5 nm Ar^+ laser beam at room temperature.

According to the usual Raman selection rules,[18] in this configuration the GaSb LO mode and the Ge optic mode are allowed, but the GaSb TO mode is forbidden. Figure 1 shows that two optic modes were observed in the alloy spectra, one near the GaSb LO mode at 234 cm^{-1} and one near the Ge optic mode at 300 cm^{-1}. The GaSb-like mode did not shift appreciably in frequency as the GaSb content was decreased; however, its intensity fell rapidly and the peak broadened considerably so that it was just discernible in the $(GaSb)_{0.27}Ge_{0.73}$ spectra. On the other hand, the frequency of the Ge-like mode decreased from 300 to 257 cm^{-1} and the intensity decreased in an approximately linear fashion as the Ge concentration was decreased from 100 to 6 mole %. The linewidth of this mode remained almost constant in the alloys.

Figure 2 shows the frequency of both the GaSb-like and Ge-like modes versus alloy concentration. The strong damping of the GaSb-like mode with decreasing GaSb concentration suggests that $(GaSb)_{1-x}Ge_x$ follows an intermediate one-

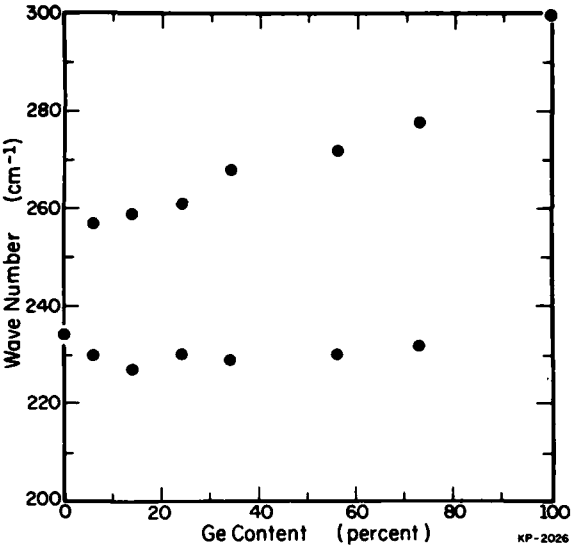

Fig. 2 Long-wavelength optical phonons in $(GaSb)_{1-x}Ge_x$ versus alloy concentration.

two mode pattern. In two-mode behavior, the optical modes of the pure crystal end-members evolve into a localized impurity mode of that constituent in the other end-member. *Intermediate* behavior occurs when creation of a distinct localized mode does not take place. In this alloy, we suggest that small concentrations of Ga and Sb in Ge do not induce localized modes in the lattice for the following reasons: (1) Ga has too small a mass difference with Ge to significantly perturb the lattice, and (2) the Ge crystal does not have a gap in its phonon density of states for creation of the gap mode associated with heavy substitutional Sb impurities ($M_{Sb}/M_{Ge} = 1.69$). Spectra taken from a 99.8 mole % Ge sample showed no evidence for Ga or Sb related local modes. In contrast, at the other end of the alloy concentration range, the Ge-like mode merged into a local mode at 257 cm^{-1} as shown in Figure 1(g). We attribute this to Ge atoms residing on Sb sites. Ge atoms on Ga sites have too small a mass difference for creation of a gap mode.

The strong broadening of the optical modes and the appearance of low-frequency modes in Fig. 1 are attributed to first-order scattering induced by the substitutional disorder in the mixed crystals. This disorder relaxes the $\vec{q} \sim 0$ Raman selection rule and allows phonons away from the zone center to become Raman active. The broad feature found near 150 cm^{-1} corresponds to the zone-edge longitudinal acoustic phonon frequencies in GaSb and Ge; structure seen at about 50 cm^{-1} matches the zone-edge transverse acoustic phonon frequencies. These observed peaks are interpreted as disorder activated longitudinal acoustic and transverse acoustic modes. The relaxation of the wave vector selection rule also affects the width and frequency of the optical phonon peaks. Off-zone center optical phonons also become Raman active due to the disorder. This broadens the peak, down-shifts the peak position in energy, and gives the peak an assymetric appearance, because of the negative slopes in the optical phonon dispersion curves of both Ge and GaSb. In spite of the substitutional disorder in these crystalline samples, the polarization dependence of the optical modes was the same as that of the zone-center modes observed in pure GaSb and Ge. The disorder-allowed acoustic phonons showed little dependence on the polarization. This is expected, since the frequencies of phonons from points such as X, L, and W are nearly the same, and a superposition of spectra would contain all Raman-active symmetries.

Spectra obtained from amorphous $(GaSb)_{1-x}Ge_x$ films are shown in Fig. 3. In amorphous materials the q-vector selection rule breaks down

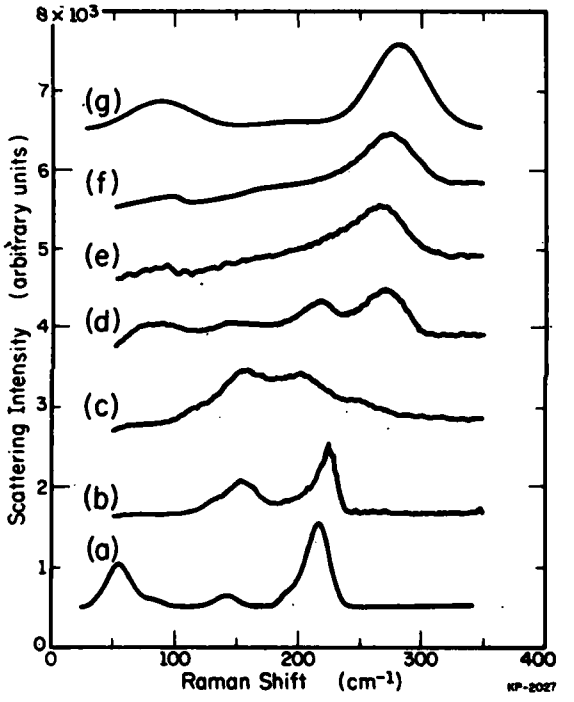

Fig. 3 Raman spectra of $(GaSb)_{1-x}Ge_x$ amorphous alloys and both end members: a) GaSb DOS, from Ref. A, convoluted with a Gaussian FWHM = 20 cm^{-1}
b) a-GaSb
c) $(GaSb)_{0.90}Ge_{0.10}$
d) $(GaSb)_{0.58}Ge_{0.42}$
e) $(GaSb)_{0.13}Ge_{0.87}$
f) a-Ge
g) Ge DOS, from Ref. B, convoluted with a Gaussian FWHM = 50 cm^{-1}

A) Marvin K. Farr, Joseph G. Taylor and S. K. Sinha, Physical Review B11, 1587 (1975).
B) G. Nelin and G. Nillson, Physical Review B5 3151 (1972).

completely, and the Raman spectra are a measure of the phonon density of states (DOS). An approximate expression for the Raman intensity $I(\omega)$ in this case is:[19]

$$I(\omega) = \sum_b C_b(\omega)\rho_b(\omega)\frac{n(\omega,T)+1}{\omega}$$

where $n(\omega,T)$ is the Bose-Einstein distribution function, $\rho_b(\omega)$ is the vibrational density of states in band b, and $C_b(\omega)$ is the coupling strength between the exciting light and the phonon band. The data in Fig. 3 are plotted as reducing Raman spectra:

$$I_R(\omega) = \frac{\omega}{n(\omega,T)+1}I(\omega) \propto \rho(\omega)$$

where the proportionality to the total density of states holds if we assume that $C_b(\omega)$ is constant with ω and b. For comparison with $I_R(\omega)$, broadened phonon densities of states for GaSb and Ge are also plotted in Fig. 3. These plots were generated by convoluting a Gaussian with the one-phonon density of states, choosing the half width of the Gaussian equal to the energy difference between the LO phonon and the cutoff of first order scattering in the amorphous spectra.[18] For alloy samples with $x < .87$, the spectra contain contributions from the DOS of both end members. The sample $(GaSb)_{.13}Ge_{.87}$ (Fig. 3e) does not display any contribution from GaSb, consistent with the one-two mode pattern postulated. The difference between the spectra and the DOS of the pure compounds, particularly in the intensities of features at low ω, is most probably due to variations in $C_b(\omega)$. There was no apparent polarization dependence of the spectra, leading to the conclusion that the amorphous films have a continuous random network-type structure.[21]

In summary, Raman scattering results on $(GaSb)_{1-x}Ge_x$ single crystals show an intermediate one-two optic phonon mode behavior. This is attributed to the lack of a localized mode by GaSb impurities in Ge. A local mode is observed in GaSb due to Ge impurities on Sb sites in the GaSb lattice. Substitutional disorder in the crystalline alloy induced substantial broadening and softening of optical modes in addition to disorder-induced scattering from the zone-edge acoustic phonons. It is, however, interesting to note that the relaxed Raman selection rules persist in the crystalline alloy films, whereas no polarization dependence was found in the amorphous forms.

Acknowledgement-The research of K. C. Cadien and J. E. Greene was supported by the Department of Energy, Division of Materials Sciences, under Contract DE-AC02-76ER01198. The research of the other authors was supported by ONR Grant N00014-80-C-0701 and JSEP Grant N00014-79-C-0424 with institutional support through the Materials Research Laboratory under Grant NSF-DMR-03523.

References

1. A.S. Barker and A.J. Sievers, Review of Modern Physics 47, s142 (1975).
2. G. Lucovsky and M.F. Chen, Solid State Communications 8, 1397 (1970).
3. Ch. Hirlimann, M. Jouanne and A. Joullie, Third International Conference on Ternary Compounds, 1977, p. 103, ed. G.D. Holah, Institute of Physics, London (1977).
4. M.A. Renucci, J. B. Renucci, and M. Cardona, Proceedings of the Second International Conference on Light Scattering in Solids, p. 326, ed. M. Balkanski, Flammarion, Paris (1971).
5. Jeffrey S. Lannin, Physical Review B16, 1510 (1977).
6. I. F. Chang and S.S. Mitra, Physical Review 172, 924 (1968).
7. G. Lucovsky, M.H. Brodsky and E. Burstein, Physical Review B2, 3295 (1970).
8. P.N. Sen and W.M. Hartmann, Physical Review B9, 367 (1974).
9. D. Schmeltzer and R. Beserman, Physical Review Letters 47, 860 (1981).
10. K.C. Cadien, A.H. Eltoukhy and J.E. Greene, Applied Physics Letters 38, 773 (1981).
11. K.C. Cadien, A.H. Eltoukhy and J.E. Greene, Vacuum 31, 253 (1981).
12. K.C. Cadien and J.E. Greene, Applied Physics Letters 40, 329 (1982).
13. S.I. Shah, K.C. Cadien and J.E. Greene, Journal of Electronic Materials 11, 53 (1982).
14. J.E. Greene, C.E. Wickersham and J.L. Zilko, Journal of Applied Physics 47, 2284 (1976).
15. C.E. Wickersham and J.E. Greene, Journal of Applied Physics 47, 4734 (1976).
16. J.E. Greene, S.A. Barnett, K.C. Cadien and M.A. Ray, Journal of Crystal Growth 56, 389 (1982).
17. C.E. Wickersham, G. Bajor and J.E. Greene, Solid State Communications 27, 17 (1978).
18. W. Hayes and R. Loudon, Scattering of Light by Crystals, p. 288. Wiley, New York (1978).
19. R. Shuker and R.W. Gammon, Physical Review Letters 25, 222 (1970).
20. J.E. Smith, Jr., M.H. Brodsky, B.L. Crowder, M.I. Nathan and A. Pinczuk, Physical Review Letters 26, 642 (1971).
21. R.J. Kobliska and S.A. Solin, Physical Review B8, 756 (1973).

Final Report on N000 14-80-C-0701

RAMAN AND OTHER OPTICAL STUDIES OF SEMICONDUCTOR ALLOYS AND SUPERLATTICES

Miles V. Klein
Department of Physics
University of Illinois at Urbana-Champaign

July, 1984

A great deal of effort has gone into the design and construction of a tandem, multipass Fabry-Perot interferometer system for use in studying bulk and surface acoustical phonons in semiconductor alloys and superlattices. The system is still not operational; work on it will continue using other research support. Improvements to an old far-infrared Fourier interferometer have been made, and the instrument will be used to study optical phonons in semiconductor alloys and superlattices in future work.

Raman studies have been made on semiconducor alloys and superlattices. One reprint and one preprint of papers on $(GaSb)_{1-x}Ge_{2x}$ metastable alloys are included. A great deal of data has been taken on the $GaSb_{1-x}As_x$ metastable alloy system, but analysis is not yet complete. An extensive study has been completed on folded acoustic and quantized optic phonons in $GaAs/Ga_{1-x}Al_xAs$ superlattices, and a paper has recently been submitted to Physical Review B. A preprint is enclosed.

RAMAN SCATTERING FROM METASTABLE

$(GaSb)_{1-x}Ge_{2x}$ ALLOYS

R. Beserman*, J.E. Greene, M.V. Klein,
T.N. Krabach, T.C. McGlinn, L.T. Romano and S.I. Shah
Materials Research Laboratory and Coordinated Science Laboratory
University of Illinois at Urbana-Champaign, Urbana, Illinois 61801

Preprint of paper to be presented at the
17th International Conference on the Physics of Semiconductors
San Francisco, California, August 6-10, 1984
Proceedings to be published by Springer-Verlag

PACS: 78.30.Gt
63.50.+x

RAMAN SCATTERING FROM METASTABLE $(GaSb)_{1-x}Ge_{2x}$ ALLOYS

R. Beserman*, J.E. Greene, M.V. Klein,
T.N. Krabach, T.C. McGlinn, L.T. Romano and S.I. Shah
Materials Research Laboratory and Coordinated Science Laboratory
University of Illinos at Urbana-Champaign, Urbana, Illinois 61801

In an extension of earlier work (1) we have used Raman Scattering to reveal structural information in mixed, metastable, crystalline $[GaSb]_{1-x}Ge_{2x}=[Ga_{1-x}Ge_x][Sb_{1-x}Ge_x]$. These alloys were deposited on GaAs substrates using a multitarget r.f. sputtering system (2).

Room temperature measurements were performed under vacuum, with the incoming laser beam perpendicular to a <100> plane, and photon polarizations along [100] directions. Figure 1 shows the Raman spectra of some of the mixed crystals and of the pure GaSb and Ge components (all normalized to same maximum peak height). When small concentrations of GaSb are introduced into Ge or small conentrations of Ge introduced into GaSb, the zone-center phonon frequency shifts, broadens, and becomes asymmetric. Figure 2 plots the frequencies versus "percent Germanium", which we define as 100x. For x<0.1 the GaSb-like phonon shows a TO-LO splitting, which cannot be detected for x>0.1. The frequency of the Ge-like optical phonon increases almost linearly with x, whereas the frequency of the GaSb-like phonon remains almost constant for $0.3 < x < 0.75$. For x>0.75 this mode can no-longer be detected, consistent with expectations for behavior of isolated substitutional Ga and Sb atoms in Ge: In low concentrations neither atom will give a local mode or a gap mode. Ge, however, does produce a local mode as a dilute impurity in GaSb.

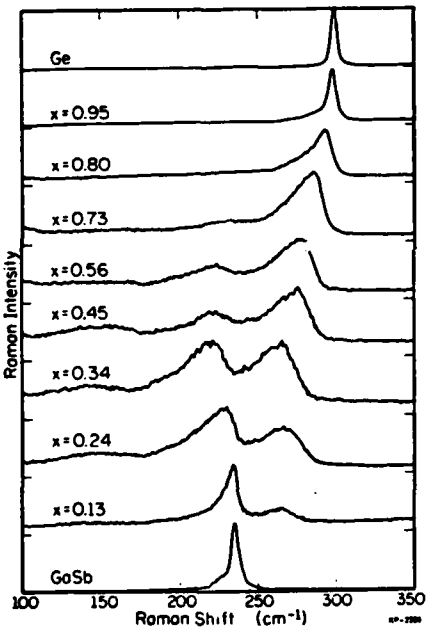

Fig. 1: Room temperature, Raman scattering of mixed $(GaSb)_{1-x}Ge_{2x}$. Scattering geometry: $z(x,y)\bar{z}$.

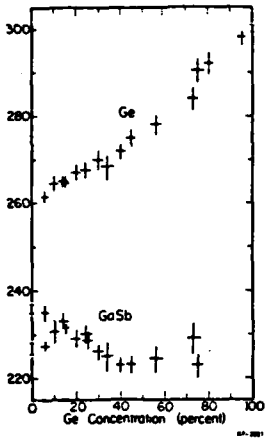

Fig. 2: Frequency dependence of peaks in $(GaSb)_{1-x}Ge_{2x}$ as a function of Ge concentration. Error bars are qualitative estimates.

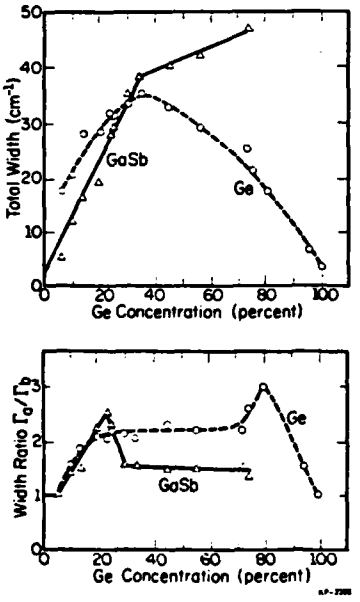

Fig. 3: Width and asymmetry at half maximum of the optical phonons.

The half widths of the optical phonons (at half-maximum) will be denoted by Γ_a and Γ_b below and above the peak, respectively. The total width $\Gamma = \Gamma_a+\Gamma_b$, and the asymmetry Γ_a/Γ_b are plotted versus x in Fig. 3. For the GaSb-like mode Γ is an increasing function of x until $x\approx0.75$, where the mode can no longer be detected. Γ for the Ge-like mode rises first linearly with (1-x), reaches a maximum for $x\approx0.35$ and then falls. The maximum values of Γ (GaSb) and Γ(Ge), 47 and 35 cm^{-1} respectively, are close to those of the pure amorphous components ($52cm^{-1}$ for a-GaSb and $47cm^{-1}$ for a-Ge). The asymmetry Γ_a/Γ_b of the GaSb-like mode increases with x until $x\approx0.25$. For $x>0.25$ Γ_a/Γ_b decreases, whereas Γ continues to increase. Similarly, the asymmetry of the Ge-like mode increases with (1-x) until $(1-x)\approx 0.20$. For $(1-x)>0.25$ the asymmetry decreases, whereas Γ continues to increase, until $(1-x)\approx0.65$. This behavior is different from that found in the quasi-binary III-V alloys $Ga_{1-x}Al_xAs$ and $Ga_{1-x}In_xAs$, where Γ_a/Γ_b is an increasing function of Γ (3) and in GaAs implanted with As^+ where Γ_a/Γ_b and Γ in samples that remain crystalline, are increasing functions of fluence (4). In these three systems Γ was never greater than about 14 cm^{-1}, and the maximum value of Γ_a/Γ_b was about 2.2.

By its very nature $[Ga_{1-x}Ge_x]$ $[Sb_{1-x}Ge_x]$ has more disorder than, say, $GaSb_{1-x}As_x$, since in the

present case both sublattices of the underlying lattice become disordered. The greater values of Γ observed here are at least partly due to this effect. An important issue is whether the non-monotonic relation of Γ_a/Γ_b to Γ is simply due to the larger amount of disorder, rather than to qualitative changes in the nature of the disorder. The abrupt changes in Γ_a/Γ_b (GaSb) near x=0.20 and Γ_a/Γ_b(Ge) near x=0.80 seem to occur over too small a change in x to be simply a quantitative effect of disorder.

In references (3) and (4) the results were analyzed using the "Spatial correlation model" which intoduces a correlation length L to account for the wave-vector relaxation (5). The contribution of phonons of finite q with frequency $\omega(q)$ and width Γ_o is accounted for by use of the following expression for the Raman line-shape:

$$I(\omega) \propto \int \exp\left(\frac{-q^2L^2}{4}\right) \frac{d^3q}{[\omega-\omega(q)]^2+[\Gamma_o/2]^2} \qquad (1)$$

$\omega(q)$ was taken to be that given by a linear chain model (3), (4). The resulting values of Γ_a, Γ_b, and Γ_a/Γ_b are increasing functions of L^{-1}. A rough extrapolation of these results to large Γ, suggests that the Γ-values in Fig. 3 imply minimum values of L of order 10Å. When a more realistic model is used for $\omega(q)$, and when both TO and LO modes are included, it is possible that for very large L^{-1} - 10^7 cm^{-1} Eq. (1) will give a line-shape with reduced asymmetry, but the change will not be an abrupt function of L^{-1}. The Γ_a/Γ_b data (Fig. 3) suggest qualitative changes in the disorder at x=0.20-0.30 and x=0.70-0.80. In $(GaAs)_{1-x}Ge_{2x}$, there is experimental and theoretical evidence for a transition from an average zincblende structure to an average diamond structure as x increases past x_c= 0.35 (6,7). X-ray diffraction data on $(GaSb)_{1-x}Ge_{2x}$ show a similar transition at x_c=0.30 (8). For $x>x_c$ there is no long-range zincblende order. The Raman results do not support the picture that site occupancy is completely random when $x>x_c$, because if that were the case we should see Raman scattering from Sb-Sb bonds. If these bonds were metallic, peaks should be seen at 115 cm^{-1} and 150 cm^{-1} (9). If the bonds were covalent, a peak would be seen at about 193 cm^{-1} [a frequency slightly scaled down from the Raman frequency in gray tin (10)]. There are no sharp features near 115, 150,

or 190 cm^{-1} that could be identified with Sb-Sb bonds. This fact together with the observation that the GaSb-like phonon continues to exist up to x=0.75 implies that Sb-Ga (and/or Sb-Ge) bonds exist, but not Sb-Sb bonds. If Sb-Ga bonds tend to be favored over Sb-Ge bonds, due to the coulomb interaction, there must be small regions of zincblende structure alternating with regions of anti-zincblende structure. The large values of L^{-1} suggested by the large values of Γ imply that these regions would be as small as 10 Å in extent. This figure is consistent with our failure to see any microstructure using a scanning transmission electron microscope with a resolution of 50 Å.

Whatever the nature of the short-range order or microstucture, the Γ_a/Γ_b data suggest that the structure changes at x=0.20-0.30 and again at x=0.70-0.80.

This work was supported by the Joint Services Electronic Program under N00014-79-C-0424, Office of Naval Research under N00014-80-C-0701, the National Science Foundation under the MRL grant DMR-80-20250, and the Department of Energy, Division of Materials Sciences under contract DE-AC02-76ER01198.

References

1. T.N. Krabach, N. Wada, M.V. Klein, K.C. Cadien, and J.E. Greene, Solid State Commun. 45, 895 (1983).
2. J.E. Greene, C.E. Wickersham, and T.L Zilco, J. Appl. Phys. 47, 2284 (1976).
3. P. Parayanthal, and F.H. Pollak, Phys. Rev. Lett. 52, 1822 (1984).
4. K.K. Tiong, P.M. Amirtharaj, F.H. Pollak and D.E. Aspnes, Appl. Phys. Lett. 44, 122 (1984).
5. H. Richter, Z.P. Wang, and L. Ley, Solid State Commun. 39, 625 (1981).
6. K.E. Newman, L. Lastras, B. Kramer, S.A. Barnett, M.A. Ray, J.D. Dow, J.E. Greene, and P.M. Raccah, Phys. Rev. Lett. 50, 1467 (1983).
7. K.E. Newman and J.D. Dow, Phys. Rev. B27, 7495 (1983).
8. S.I. Shah and B. Kramer, unpublished work.
9. J. Hohne, U. Wenning, H. Shultz, and S. Hufner, Z. Phys. B27, 297, (1977).
10. C.J. Buchenauer, M. Cardona, and F.H. Pollak, Phys. Rev. B3, 1243 (1970).

* Permanent Address: Solid State Institute, Physics Dept., Technion, Institute of Technology, Haifa, Israel.

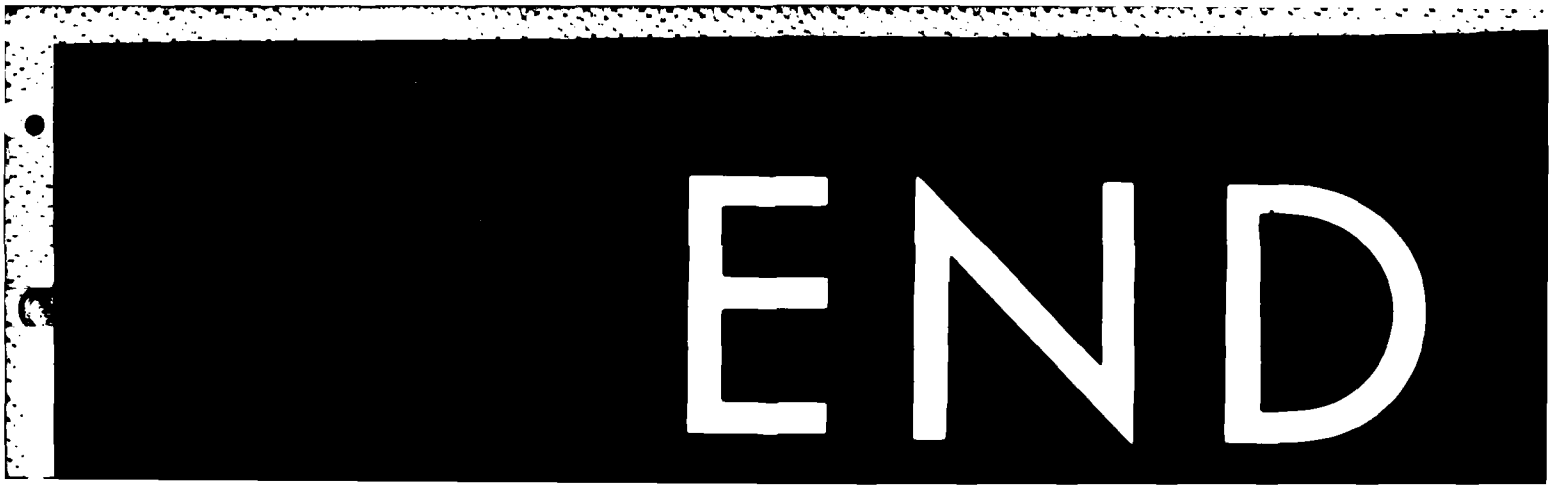
END